

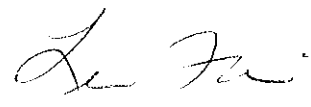
A SIMPLE MODEL OF OSCILLATORS COUPLED THROUGH FLUID:
EFFECT OF REYNOLDS NUMBER

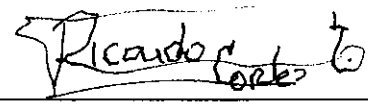
AN ABSTRACT

SUBMITTED ON THE FIFTH DAY OF AUGUST, 2016
TO THE DEPARTMENT OF MATHEMATICS
OF THE SCHOOL OF SCIENCE AND ENGINEERING OF
TULANE UNIVERSITY
IN PARTIAL FULFILLMENT OF THE REQUIREMENTS
FOR THE DEGREE OF
DOCTOR OF PHILOSOPHY
BY


SHANSHAN JIANG

APPROVED: _____


LISA FAUCI
CHAIR


RICARDO CORTEZ


CHRISTINA HAMLET


JAMES HYMAN


MORRIS KALKA

Abstract

We examine the hydrodynamic interaction of two oscillators in a 2D fluid driven by a geometric switch. Motivated by the work of Kotar et al (PNAS, 107:17, 2010), the colloidal oscillators are modeled by circular membranes that support tensile forces on their boundary and forces due to an external trap that switches between two spatial positions, depending upon the position of the oscillator. Numerical experiments are performed using an immersed boundary framework where the viscous, incompressible fluid is governed by either the inertia-free Stokes equations or the full Navier-Stokes equations. In the Stokes case, the anti-phase state is stable and the in-phase state is not. However, when a slight amount of inertia is added, we find that both states are stable to small perturbations. For higher, but still moderate Reynolds numbers we find that the anti-phase state is unstable and all perturbations tend to in-phase oscillations a dramatic change from zero Reynolds number.

A SIMPLE MODEL OF OSCILLATORS COUPLED THROUGH FLUID:
EFFECT OF REYNOLDS NUMBER

A DISSERTATION
SUBMITTED ON THE FIFTH DAY OF AUGUST, 2016
TO THE DEPARTMENT OF MATHEMATICS
OF THE SCHOOL OF SCIENCE AND ENGINEERING OF
TULANE UNIVERSITY
IN PARTIAL FULFILLMENT OF THE REQUIREMENTS
FOR THE DEGREE OF
DOCTOR OF PHILOSOPHY
BY


SHANSHAN JIANG


APPROVED: _____


LISA FAUCI
CHAIR


RICARDO CORTEZ


CHRISTINA HAMLET


JAMES HYMAN


MORRIS KALKA

©Copyright by Shanshan Jiang, 2016

All Rights Reserved

Acknowledgement

I am particularly thankful to my advisor, Dr. Lisa Fauci, for her guidance and support, great ideas and permanent assistance with my research, and also being a good consultant for life. I would like to thank Drs. Ricardo Cortez, Mac Hyman and Christina Hamlet for their helpful insights and assistance in my research. I would also like to thank Dr. Morris Kalka for serving on my dissertation committee.

I would like to express my thanks to Dr. Franz Hoffmann, Elham (Ellie) Ahmadi, Qiang Yang, Mr. Forest Mannan and other graduate students in Math Department, for their mathematical advice, friendship and constant support in many regards. It is my great pleasure to share these years with you guys in New Orleans.

I would like to thank the faculty and staff in Math Department, for whom I received lots of help and advice, and also the great patience in answering my question.

And finally, I thank my parents for their love, support encouragement, and everything else during all my life.

List of Tables

3.1	Relative position of two immersed bodies in critical times for anti-phase state.	26
3.2	Relative position of two immersed bodies in critical times for in-phase state.	34
4.1	The default setting for dimensionless parameters used in Stokes flow cases.	42
4.2	The temporal period computed with the choosing of different blob size. Using the same set of parameters, the half temporal period computed using Oseen approximation is 1.8435. Here ϵ is the blob size for Stokeslet, and T represents the half temporal period.	42
4.3	The half temporal period comparison between regularized Stokeslets and Oseen Approximation, with different dt	43
4.4	The setting of trap position.	48
4.5	The initial setting of four cases.	49
4.6	The setting of trap position.	52
4.7	The initial setting of four cases.	52
4.8	The setting of trap position.	56
5.1	The default setting for dimensionless parameters used in Navier-Stokes cases.	67

5.2	The setting of trap position.	73
5.3	The initial setting of active traps and oscillators positions. IB_i indicates the centroid of immersed body i , $i = 1, 2$	73

List of Figures

1.1	Examples of synchronization of oscillators at the microscale.	2
(a)	Sperm swimming. [1] D Woolley et al., A study of synchronization between the flagella of bull spermatozoa, with related observations. J. of Experimental Biology, 212(14):2215-2223, 2009.	2
(b)	Cilia beating in lung. Courtesy of Charles Daghljan, Dartmouth College.	2
1.2	High-speed imaging probe of the beating pattern of the flagella. [2]Goldstein, Raymond E. et al., Noise and Synchronization in Pairs of Beating Eukaryotic Flagella, Phys. Rev. Lett., doi = 10.1103/PhysRevLett.103.168103	3
1.3	Diagram of normal cilia beating cycle. The beating cycle is characterized by an active beating stroke (black) and a recovery stroke (grey) [3]	3
2.1	Snapshots of single oscillator. The red circle is the immersed body, and the blue circle is the active trap.	7
2.2	The physical system of two oscillators. (A) illustrates the setting of two oscillators. (B) illustrates a single oscillator movement. (C) is a sequence of snapshots of two oscillators. The long term behavior is an anti-phase state. Taken from [4].	8

3.1	Point force $\mathbf{f}_0 = (4\pi\mu, 0)$ exerted at $\mathbf{x}_0 = (10^{-5}, 0)$. Singularity of velocity field happens when we use analytic solution. (a) shows the relationship between r and u_1 (the velocity in x -direction). As $r \rightarrow 0$, $u_1 \rightarrow \infty$. (b) shows the velocity field of the domain $[-1, 1] \times [-1, 1]$. We replace the velocity at $(0, 0)$ by $(0, 0)$ to see the velocity field everywhere.	15
(a)	15
(b)	15
3.2	Blob function δ_ϵ with $\epsilon = 0.2$ and $\epsilon = 0.5$.	16
3.3	B_ϵ and G_ϵ corresponding to $\epsilon = 0.2$ and $\epsilon = 0.5$.	16
(a)	G_ϵ	16
(b)	B_ϵ	16
3.4	Velocity field generated using equation 3.4 and 3.5 by force $\mathbf{f}_0\delta_\epsilon(\mathbf{x}_0)$ where $\mathbf{f}_0 = (4\pi\mu, 0)$ and $\mathbf{x}_0 = (0, 0)$, with different ϵ ($\epsilon = 0.2$ and $\epsilon = 0.5$). The red arrow shows the direction and magnitude of the force, the the blue arrows are the plotted velocity field.	17
(a)	$\epsilon = 0.2$	17
(b)	$\epsilon = 0.5$	17
3.5	Velocity field generated by a point force $(3\pi\mu, \pi\mu)$ acting on the point $(0, 0)$ with spatial periodicity $L = 0.5$ in x -direction.	19
3.6	Velocity on y -axis generated by a point force $(4\pi\mu, 0)$ acting on $(0, 0)$. Here $\epsilon = 0.01$.	20
3.7	The initial and end figure for the computed period. Blue circle is the active trap, the light blue one is the inactive trap, and the red one is the oscillator. At $t = 0$, the oscillator is farthest away from the trap and moving left, it switches moving direction at $t = T$, when the threshold distance ξ is reached.	22

3.8	Relative position of the oscillators at the critical times, perturbed anti-phase case.	27
3.9	Relative position of the oscillators at the critical times, perturbed in-phase case.	33
(a)	Case (1), x_1 switches direction first.	33
(b)	Case (2), x_2 switches direction first.	33
4.1	Illustration graph for single oscillator system.	40
4.2	The temporal period comparison between regularized Stokeslet and Oseen Approximation, with different distance between traps λ	43
4.3	The temporal period comparison between regularized Stokeslet and Oseen Approximation, with different ξ	44
4.4	The temporal period comparison between regularized Stokeslet and Oseen Approximation, with different trapping stiffness κ	45
4.5	The spatial period is same as oscillating direction. Here L is the spatial periodicity.	45
4.6	The temporal period comparison between singly periodic oscillators case (a) and single oscillator in Stokes free space.	46
4.7	The spatial period is orthogonal to the oscillating direction. Here L is the spatial periodicity.	47
4.8	The temporal period comparison between singly periodic oscillators case (b) and single oscillator in Stokes free space.	48
4.9	Snapshot of two oscillators coupling through fluid. Initially set to be exact in-phase state, and the coupling goes to anti-phase.	50
4.10	The shifted centroid plot of four cases of parallel placed oscillators. All four cases go to anti-phase.	51
(a)	Exact in-phase initial setting.	51
(b)	Perturbed in-phase initial setting.	51

(c)	Exact anti-phase initial setting.	51
(d)	Perturbed anti-phase initial setting.	51
4.11	Coupling indicator for four cases, parallel placed oscillator.	51
4.12	The shifted centroid plot of four cases of vertical placed oscillators.	
	The exact in-phase case keeps in-phase, all others go to anti-phase. . .	53
(a)	Exact in-phase initial setting.	53
(b)	Perturbed in-phase initial setting.	53
(c)	Exact anti-phase initial setting.	53
(d)	Perturbed anti-phase initial setting.	53
4.13	Coupling indicator for four cases, vertical placed oscillator.	53
4.14	Snapshots of perturbed in-phase case.	54
4.15	Snapshot of perturbed in-phase case at $t = 1$ for a larger domain. . .	55
4.16	Trajectory of oscillators with different d . Here the trajectory is shown	
	in blue, and the possible trap positions are shown in red.	57
4.17	Coupling indicator for different d . All three cases go close to anti-phase.	58
4.18	Snapshots of two oscillators placed in horizontal-vertical group. . . .	58
4.19	Snapshot of two oscillators placed in horizontal-vertical group at $t = 1$.	59
4.20	Illustration figure of three oscillators with random initial condition. .	59
4.21	Shifted centroid plot for three oscillators.	60
4.22	Coupling indicator Q . $Q_{(1,3)}$ greater than zero shows the two lateral	
	oscillators tend to go in-phase, while $Q_{(1,2)}$ and $Q_{(2,3)}$ less than zero	
	shows the middle oscillator tends to go anti-phase to the lateral ones.	60
4.23	Shifted centroid plot for three oscillators.	61
4.24	Coupling indicator Q . $Q_{(1,3)} = -1$ shows the two lateral oscillators	
	are exact anti-phase, while $Q_{(1,2)}$ and $Q_{(2,3)}$ around zero indicates the	
	middle oscillator just passively move with the fluid.	61
5.1	Centroid plot of single oscillator with different N_b	68

5.2	Single oscillator in Navier-Stokes fluid.	70
5.3	Single oscillator in Navier-Stokes fluid, with the adjusted force. Tem- poral period comparison between cases of Navier-Stokes and free space Stokes.	71
5.4	For $Re = 40$, the deformation of the elastic body is observed.	72
5.5	Both in-phase state and anti-phase state keep in-phase / anti-phase. ($\rho = 10$)	73
	(a) Exact in-phase initial setting. $Re = 0.08$	73
	(b) Exact anti-phase initial setting. $Re = 0.05$	73
5.6	Centroid plot for perturbed in-phase state.	75
	(a) $\rho = 10$, $Re = 0.06$	75
	(b) $\rho = 100$, $Re = 0.43$	75
5.7	Q plot.(a) shows Q plot for $\rho = 10$ ($Re = 0.06$) and $\rho = 100$ ($Re =$ 0.43). (b) shows Q plot for $10 \leq \rho \leq 100$ ($0.06 \leq Re \leq 0.43$), with difference of 5 in ρ between each simulation.	75
	(a)	75
	(b)	75
5.8	Blue stars indicate that in-phase state was stable and red circles indi- cate that in-phase state was unstable.	76
5.9	Perturbed anti-phase state.	77
	(a) $\rho = 10$, $Re = 0.06$	77
	(b) $\rho = 100$, $Re = 0.40$	77
5.10	Q plot. (a) shows Q plot for $\rho = 10$ ($Re = 0.06$) and $\rho = 100$ ($Re =$ 0.40). (b) shows Q plot for $10 \leq \rho \leq 100$ ($0.06 \leq Re \leq 0.40$), with difference of 5 in ρ between each simulation.	78
	(a)	78
	(b)	78

5.11 Blue star indicates anti-phase unstable, red circle indicates anti-phase stable.	78
5.12 For $Re = 40.1$, the coupling state of two oscillators is in-phase, and the deformation is observed.	80
5.13 Illustration graph for four oscillators coupling.	81
5.14 Centroid plot for four oscillators. $Re = 0.14$, $\rho = 20$	81
5.15 Snapshots of four oscillators coupled through fluid.	82
5.16 Random placed oscillators become in-phase at the end of simulation time.	82

Contents

Acknowledgement	ii
List of Tables	iii
List of Figures	v
1 Introduction	1
2 Model Setting	6
2.1 Oscillator Model	6
2.2 Mathematical Model	7
2.3 In/anti-phase indicator	10
3 Analytical Study of Stokes Case	12
3.1 Free Space Stokes Case	12
3.2 Singly Periodic Stokes Case	17
3.3 Oseen Tensor Approximation	20
3.3.1 Single Oscillator	20
3.3.2 Two Oscillators	22
4 Numerical Simulation of Stokes Case	40
4.1 Numerical Method	40
4.2 Single Oscillator Simulation	42

4.3	Two Oscillators	48
4.4	Multiple Oscillator	57
5	Navier Stokes Flow	62
5.1	Numerical Background	62
5.1.1	The Immersed Boundary Method	62
5.2	Computation Steps	64
5.3	Numerical Simulation for a Single Oscillator.	66
5.3.1	Convergence study	66
5.3.2	Inertia affects the oscillator motion	69
5.3.3	Modify Re by changing fluid density ρ	69
5.3.4	High Re case	71
5.4	Numerical Simulation for Two Oscillators	71
5.4.1	Exactly in-phase / anti-phase case	72
5.4.2	Perturbed in-phase / anti-phase case	72
5.4.3	High Re case	79
5.5	Multiple Oscillators	79
6	Conclusion and Future Work	83
6.1	Conclusion	83
6.1.1	Stokes fluid	83
6.1.2	Navier-Stokes fluid	84
6.2	Future Work	85
	References	86

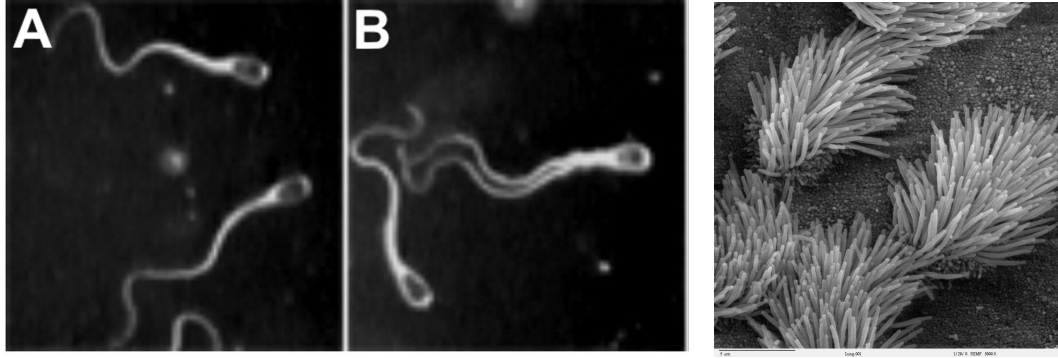
Chapter 1

Introduction

The goal of this thesis is to study the hydrodynamic interaction of oscillators that are driven by a geometric switch. We focus on how inertia changes the synchronization state of the coupling of oscillators.

The motion and trajectory of small objects swimming in fluid is a classical problem in biological fluid dynamics. In 1971, Berg [5] set up an apparatus to observe the locomotion of bacteria. Bacteria swim by rotating their flagella [6]. If there are several flagella per cell, the rotation synchronizes. Such synchronization is commonly seen at the microscale. Examples of interacting organisms in a fluid at the microscale include flagellar swimming [2, 7, 8] and ciliary beating [9, 10]. Woolley et al. in [1] showed the synchronization of flagella of two bull sperm (about $55\ \mu\text{m}$) as they approach close to each other. The paired sperm exhibit rises in conjoint beat frequency and swimming velocity. As seen in Figure 1.1(a), two sperm, initially not synchronized (A), begin to synchronize to an in-phase oscillation (B). Goldstein et al. [2] observed that two flagella (about $12\ \mu\text{m}$) of *Chlamydomonas* beat in an anti-phase pattern, as seen in Fig 1.2. Coordinated oscillations also occur in arrays of respiratory cilia in the lung (about $4\text{-}7\ \mu\text{m}$) as shown in Figure 1.1(b). Mammalian sperm cells have a single flagellum attached to a cell body, while the *Chlamydomonas* algal cell has

two flagella. Respiratory cilia in human airways form dense arrays. The internal structure of both cilia and flagella in eukaryotic cells is conserved, and the action of dynein molecular motors on microtubules gives rise to filament oscillation.



(a) Sperm swimming. [1] D Woolley et al., A study of synchronization between the flagella of bull spermatozoa, with related observations. J. of Experimental Biology, 212(14):2215-2223, 2009. (b) Cilia beating in lung. Courtesy of Charles Daghljan, Dartmouth College.

Figure 1.1: Examples of synchronization of oscillators at the microscale.

Several simple models have been proposed to study the interaction of flagellar motion. Here we use a simple oscillator model [11]. A ciliary beat, characterized by a power and recovery stroke, as seen in Fig 1.3, is modeled by the oscillation of a bead in the oscillator model.

The coupling of multiple oscillators is well-studied. Hough and Ou-Yang studied the coupling of two particles coupled through fluid with each trapped in a quadratic potential well, both experimentally and analytically [12]. By setting one of the trapped particle into forced oscillation using oscillating optical tweezers, they showed that the in-phase and anti-phase motion of both particles in the traps is a function of driven oscillating frequency. Extended work has been done by Herrera-Velarde et al. in [13] by adding a third body in the colloidal array. They showed that by adding a third-body, the auto-correlation functions show a slower decay, while the cross-correlation ones exhibit a temporal shift and a weaker amplitude.

In 2008, Kotar et al. [14] conducted experiments and a simple model with three

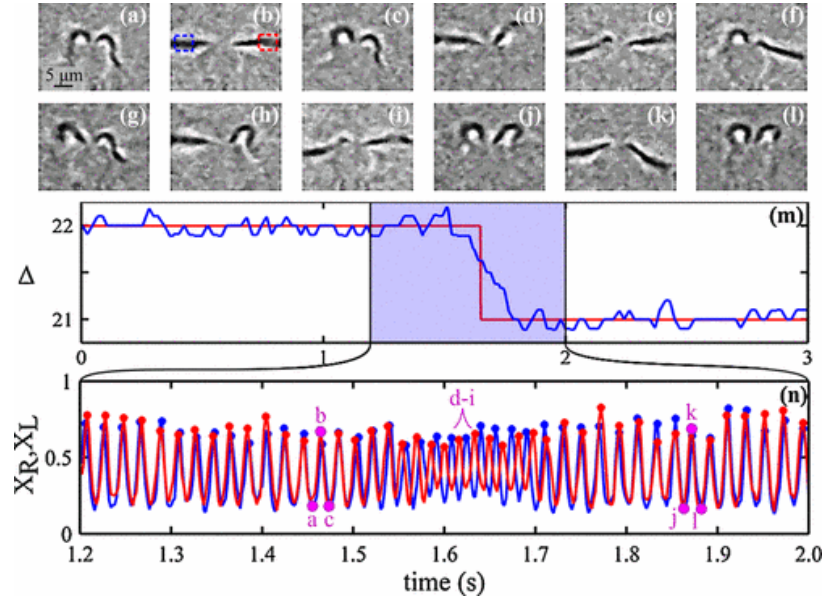


Figure 1.2: High-speed imaging probe of the beating pattern of the flagella. [2]Goldstein, Raymond E. et al., Noise and Synchronization in Pairs of Beating Eukaryotic Flagella, Phys. Rev. Lett., doi = 10.1103/PhysRevLett.103.168103

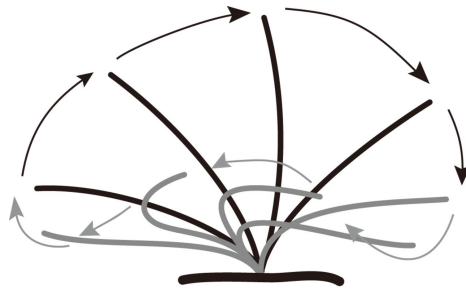


Figure 1.3: Diagram of normal cilia beating cycle. The beating cycle is characterized by an active beating stroke (black) and a recovery stroke (grey) [3]

elastic particles placed in a line. The two lateral elastic particles oscillate due to the switching of an optical trap between two positions respectively, and the central particle stays at rest. They showed that the system is able to generate flow. In 2010, Kotar et al. [4] studied two oscillators placed next to each other with hydrodynamic interaction. Their analysis shows that in a Stokes fluid, the two oscillators can synchronize in-phase or anti-phase, and the anti-phase state is stable. Lhermerout et al. studied the coupling of two oscillators with different orientation in [15]. They have shown the analysis of the mean configurations (position and angles) of driven oscillators to predict the main properties of the steady state of the collective system undergoing geometric switch oscillations. Particles oscillating on the vertices of planar regular polygons have also been studied in [16–18]. Damet et al. have shown in [17] that two particles or polygonal arrays of four or more colloids synchronize with the nearest neighbors that are in anti-phase, while three equally spaced colloids synchronize in-phase. Bruot et al. in [19] show that the type of trap driven potential affects the synchronization of oscillators coupled through fluid. Positive curvature of the potential well drives the system to anti-phase synchronization, while negative curvature drives it to in-phase synchronization. When zero curvature occurs, the two oscillators do not synchronize.

Most studies of hydrodynamic coupling have been done in a Stokes fluid, where inertial effects are neglected. Theers and Winkler studied the time dependent version in [20]. They used the coupled rotor model to study the hydrodynamic interaction, and showed the linear unsteady acceleration term in the Navier-Stokes equation leads to synchronization of the rotational motion.

We extend the hydrodynamic interaction to a Navier-Stokes fluid and study how inertia affects the coupling of oscillators. We also compare our simulations with the previous result.

In Chapter 2, we discuss the setup of the model system in detail. In Chapter 3, we

study the coupling of oscillators in a Stokes fluid. Our analysis shows that in the case of two oscillators placed next to each other, when we assume the deformation of the oscillators is negligible, both the in-phase state and anti-phase state are equilibria. The in-phase state is unstable and anti-phase state is stable. This result is consistent with the work in [4]. In Chapter 4, we numerically computed the coupling of oscillators in Stokes flow, using both free-space and singly periodic boundary conditions. We validate the model by computing temporal oscillation period as functions of model parameters. Furthermore, we study the coupling of multiple oscillators placed in different positions. In Chapter 5, we study the coupling of oscillators in a Navier-Stokes fluid. Using an immersed boundary method to simulate the oscillators, we have demonstrated that both in-phase and anti-phase states are equilibria, and both are stable to small perturbations. As the Reynolds number gets larger, the attraction region of anti-phase gets smaller, while the attraction region of in-phase gets larger.

Chapter 2

Model Setting

2.1 Oscillator Model

Experimentally, a colloidal particle has been used to model a cilium, and optical traps [21] are used to generate driving potential wells. In this thesis, the colloidal particle is modeled in $2D$ by a circular membrane that supports tensile and bending forces on its boundary. The particle experiences force due to an external trap that switches between two spatial positions. The particle is driven by a trap generating a harmonic potential well. The particle experiences a force towards the trapping position until the distance between the center of the immersed body and the trap reaches a threshold. When the threshold distance is reached, the trap position is switched and the oscillator moves towards the other trap position. Snapshots of such an oscillation is shown in Figure 2.1. The red circle is the immersed body, and the blue circle is the active trap. Starting from time $t = 0$, the immersed body is attracted by the trap on the right, and kept moving right. Note that at $t = 0.6$, the immersed body is very close to the active trap. When it reaches the threshold distance to the right activating trap at $t = 0.73$, the trap switches position to the left immediately, and we observe in the next figure, at $t = 0.8$, the immersed body moves left. The

moving direction of the oscillator remains fixed until the body reaches the threshold distance of the left trap at $t = 1.64$, the trap switches to right again as seen in $t = 1.8$.

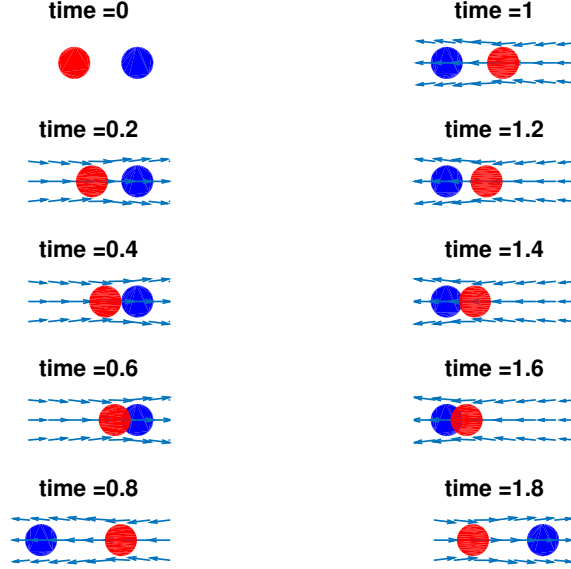
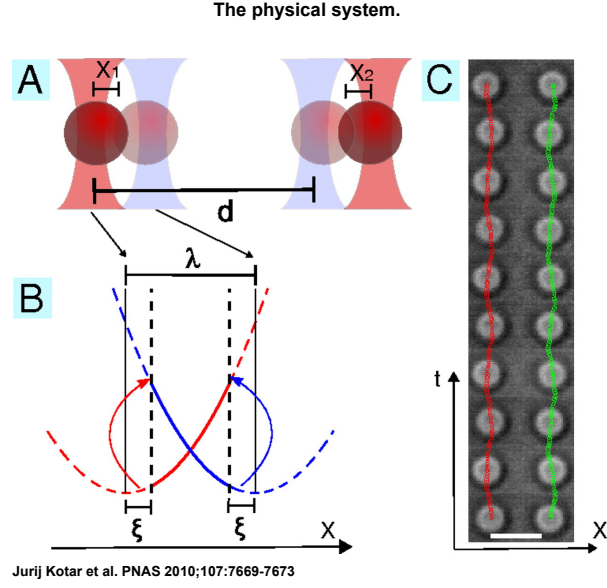


Figure 2.1: Snapshots of single oscillator. The red circle is the immersed body, and the blue circle is the active trap.

Figure 2.2(b), taken from [4], shows the structure of a single oscillator. The distance between two possible positions of the trap for a single oscillator is λ , and the threshold distance for trap switching is ξ . In the study of the coupling of two oscillators, we consider first the case when two oscillators are placed next to each other. The distance between their centers is d (shown in Fig 2.2 (A)). Snapshots of experimental data are shown in Fig 2.2 (C). Here we note that as time increases, the colloidal particles show an anti-phase oscillation.

2.2 Mathematical Model

The mathematical model of an oscillator coupled to an incompressible fluid is formulated below.



©2010 by National Academy of Sciences

PNAS

Figure 2.2: The physical system of two oscillators. (A) illustrates the setting of two oscillators. (B) illustrates a single oscillator movement. (C) is a sequence of snapshots of two oscillators. The long term behavior is an anti-phase state. Taken from [4].

1. Fluid Motion.

The motion of fluid is described by the Navier-Stokes equation (2.1) with incompressibility condition (2.2).

$$\rho \left(\frac{\partial \mathbf{u}}{\partial t} + (\mathbf{u} \cdot \nabla) \mathbf{u} \right) = -\nabla p + \mu \Delta \mathbf{u} + \sum_{k=1}^M \mathbf{f}_k \quad (2.1)$$

$$\nabla \cdot \mathbf{u} = 0 \quad (2.2)$$

Here t is time, ρ is the density of the fluid, μ is the dynamic viscosity of the fluid, \mathbf{u} is the velocity, p is pressure and \mathbf{f}_k is the external force per unit area exerted on the fluid by the k^{th} oscillator. These equations hold in a domain D . We will consider both singly periodic and doubly periodic boundary condition in D . In addition, in the Stokes case we will take $D = \mathbb{R}^2$.

2. Body-fluid Interaction.

The interaction between the immersed body and the fluid is described by (2.3) and (2.4). Here we assume the fluid and the immersed body share the same density and also the no-slip condition at the interface between the immersed body and the fluid is satisfied.

$$\mathbf{f}_k(\mathbf{x}, t) = \int_{\Gamma_k} \mathbf{F}_k(s, t) \delta(\mathbf{x} - \mathbf{X}_k(s, t)) ds \quad (2.3)$$

$$\mathbf{U}_k(s, t) = \mathbf{u}(\mathbf{X}_k(s, t), t) = \int_D \mathbf{u}(\mathbf{x}, t) \delta(\mathbf{x} - \mathbf{X}_k(s, t)) d\mathbf{x} \quad (2.4)$$

Here $\mathbf{X}_k(s, t)$, $\mathbf{U}_k(s, t)$, $\mathbf{F}_k(s, t)$ represent the position of the k^{th} immersed body, velocity of the immersed body and force exerted by the immersed body respectively, where s is an arclength parameter. The two-dimensional Dirac-delta function is denoted by δ .

3. Force.

The forces exerted on the immersed body are derived from an energy function (2.5). For a single oscillator, the energy function consists of two parts (2.6): trap energy generated from the harmonic well and the membrane energy from the immersed body itself. The membrane energy consists of tensile energy and bending energy (2.7).

For a single oscillator, we suppress the subscript k and write:

$$\mathbf{F} = -\frac{\partial E}{\partial \mathbf{X}} \quad (2.5)$$

$$E = E_{membrane} + E_{trap} \quad (2.6)$$

$$E_{membrane} = \int_{\Gamma} \left(S_{m1} \left(\left\| \frac{\partial \mathbf{X}(s, t)}{\partial s} \right\| - 1 \right)^2 + S_{m2} \left(\left\| \frac{\partial^2 \mathbf{X}(s, t)}{\partial s^2} \right\| - \tilde{c} \right)^2 \right) ds \quad (2.7)$$

$$E_{trap} = \int_{\Gamma} S_t \|\mathbf{X}(s, t) - \mathbf{T}_{active}\|^2 ds \quad (2.8)$$

Here \tilde{c} is chosen so that the curvature of membrane is that of a circle of radius a . S_{m1} , S_{m2} , S_t are the tensile stiffness, bending stiffness, and trap stiffness respectively, and $\mathbf{T}_{active} = \mathbf{T}_{\alpha}$ represents the position of the active trap, where \mathbf{T}_1 , \mathbf{T}_{-1} are the possible positions of the trap and $\alpha \in \{-1, 1\}$ is a configuration-coupled variable that switches at the trigger position. Formally, the switch condition can be written as

$$\dot{\alpha} = \pm 2\delta(t - t^{\pm})$$

where t^{\pm} is such that $\mathbf{X}(s, t^{\pm}) - \mathbf{T}_{active} = \pm \xi$ and δ is the one-dimensional Dirac delta function. As a function of time, α appears as a step function, which is set by the dynamics of $\mathbf{X}(s, t)$.

2.3 In/anti-phase indicator

When more than one oscillator is moving in the fluid, we would like to study the coupling of them quantitatively.

We define \mathbf{x}_i by

$$\mathbf{x}_i = \mathbf{X}_i - \frac{1}{2}(\mathbf{T}_{i,1} + \mathbf{T}_{i,-1})$$

$$\mathbf{x}_i = x_i \mathbf{e}_i$$

which is the relative position of oscillator i to the center of two possible trap positions related to it, $\mathbf{e}_i = \mathbf{x}_i / \|\mathbf{x}_i\|$. We quantify the phase correlation between oscillator i and j by (2.9)

$$Q_{i,j}(t_0, t_1) = \frac{\langle x_i, x_j \rangle}{\|x_i\| \|x_j\|} \quad (2.9)$$

Where

$$\langle x_i, x_j \rangle = \int_{t_0}^{t_0+t_1} x_i(t) x_j(t) dt.$$

t_0 is where the viewing window to quantify coupling state starts, and t_1 is the length of the viewing window. If $Q_{i,j} = 1$, the two oscillators are exactly in-phase. When they are exactly anti-phase, $Q_{i,j} = -1$.

Chapter 3

Analytical Study of Stokes Case

In this section, we study the behavior of oscillators in Stokes flow. When the Reynolds number is very small (in the order of 10^{-4}), we approximate the Navier-Stokes equations by the linearized version, the Stokes equations.

$$\begin{aligned} -\nabla p + \mu \Delta \mathbf{u} + \mathbf{f} &= 0 \\ \nabla \cdot \mathbf{u} &= 0 \end{aligned}$$

3.1 Free Space Stokes Case

Since the Stokes equations are linear, the velocity field generated by a group of point forces can be computed by adding the velocity field generated by each individual point force. The point force \mathbf{f}_0 centered at point \mathbf{x}_0 can be written as $\mathbf{f}_0 \delta(\mathbf{x} - \mathbf{x}_0)$ where δ is the Dirac-delta function. Given a point force acting on the fluid, the velocity anywhere in the unbounded fluid domain can be computed analytically.

In the point force case, we have

$$0 = -\nabla p + \mu \Delta \mathbf{u} + \mathbf{f}_0 \delta(\mathbf{x} - \mathbf{x}_0) \tag{3.1}$$

Take the divergence of equation (3.1), and combine with the incompressibility condition of the fluid

$$\nabla \cdot \mathbf{u} = 0.$$

We have

$$0 = -\Delta p + \nabla \cdot (\mathbf{f}_0 \delta(\mathbf{x} - \mathbf{x}_0)),$$

which is

$$\Delta p = \mathbf{f}_0 \cdot \nabla \delta(\mathbf{x} - \mathbf{x}_0).$$

Let G be the Green's function that satisfies

$$\Delta G(\mathbf{x}) = \delta(\mathbf{x})$$

Then

$$p(\mathbf{x}) = \mathbf{f}_0 \cdot \nabla G(\mathbf{x} - \mathbf{x}_0).$$

Plug p back into (3.1), we have

$$\mu \Delta \mathbf{u}(\mathbf{x}) = \nabla(\mathbf{f}_0 \cdot \nabla G(\mathbf{x} - \mathbf{x}_0)) - \mathbf{f}_0 \Delta G(\mathbf{x} - \mathbf{x}_0)$$

Let B solve

$$\Delta B(\mathbf{x}) = G(\mathbf{x}),$$

Then

$$\mu \mathbf{u}(\mathbf{x}) = ((\mathbf{f}_0 \cdot \nabla) \nabla - \mathbf{f}_0 \Delta) B(\mathbf{x} - \mathbf{x}_0)$$

This is the explicit solution of the Stokes equations.

In the 2D case, we have

$$B(r) = \frac{r^2}{8\pi} \left(\log(r) - \frac{3}{2} \right)$$

and

$$G(r) = \frac{1}{2\pi} \left(\log(r) - \frac{1}{2} \right),$$

and the velocity is given by

$$4\pi\mu u_1(\mathbf{x}) = f_1 \left(\frac{\hat{x}_1^2}{r^2} - \log(r) \right) + f_2 \left(\frac{\hat{x}_1 \hat{x}_2}{r^2} \right) \quad (3.2)$$

$$4\pi\mu u_2(\mathbf{x}) = f_2 \left(\frac{\hat{x}_2^2}{r^2} - \log(r) \right) + f_1 \left(\frac{\hat{x}_1 \hat{x}_2}{r^2} \right) \quad (3.3)$$

Here $\mathbf{f}_0 = (f_1, f_2)$ is the external force acting on the point \mathbf{x}_0 , $(\hat{x}_1, \hat{x}_2) = \mathbf{x} - \mathbf{x}_0$, $r = |\mathbf{x} - \mathbf{x}_0|$, \mathbf{x} is the point where the velocity is evaluated.

Equation (3.2) and (3.3) are defined everywhere except at the point where the force is exerted, in which case the singularity occurs. As $r \rightarrow 0$, the velocity goes to infinity.

An example is illustrated in Fig 3.1. A point force $\mathbf{f}_0 = (4\pi\mu, 0)$ is exerted at $\mathbf{x}_0 = (10^{-5}, 0)$. Fig 3.1 (a) shows the velocity in the x -direction on x -axis. When we plot the velocity field in Fig 3.1(b), we change the velocity evaluated at $(0, 0)$ to be $(0, 0)$ to see the detailed velocity field.

In order to remove the singularity of the velocity field, we use the method of regularized Stokeslets derived by Cortez [22]. Instead of the point force assumption using δ -function, we choose a δ_ϵ -function to represent a concentrated force applied over a small non-zero area. The corresponding G_ϵ and B_ϵ satisfy

$$\Delta G_\epsilon(r) = G_\epsilon''(r) + \frac{1}{r} G_\epsilon'(r) = \delta_\epsilon(r)$$

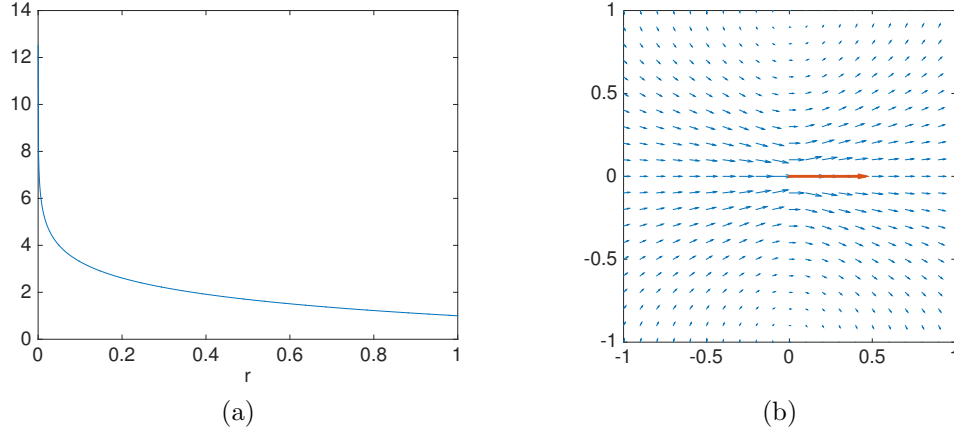


Figure 3.1: Point force $\mathbf{f}_0 = (4\pi\mu, 0)$ exerted at $\mathbf{x}_0 = (10^{-5}, 0)$. Singularity of velocity field happens when we use analytic solution. (a) shows the relationship between r and u_1 (the velocity in x -direction). As $r \rightarrow 0$, $u_1 \rightarrow \infty$. (b) shows the velocity field of the domain $[-1, 1] \times [-1, 1]$. We replace the velocity at $(0, 0)$ by $(0, 0)$ to see the velocity field everywhere.

$$\Delta B_\epsilon(r) = B_\epsilon''(r) + \frac{1}{r}B_\epsilon'(r) = G_\epsilon(r).$$

For example, in $2D$, we can use

$$\delta_\epsilon(r, \epsilon) = \frac{2\epsilon^4}{\pi(r^2 + \epsilon^2)^3},$$

$$G_\epsilon = \frac{1}{4\pi} \left(\log(r^2 + \epsilon^2) - 1 - \frac{\epsilon^2}{r^2 + \epsilon^2} \right),$$

$$B_\epsilon = \frac{1}{8\pi}(r^2 + \epsilon^2) \left(\frac{1}{2} \log(r^2 + \epsilon^2) - \frac{3}{2} \right).$$

The velocity field is:

$$4\pi\mu u_1 = \frac{f_1 \hat{x}_1^2 + f_2 \hat{x}_1 \hat{x}_2}{r^2 + \epsilon^2} - f_1 \left(\frac{1}{2} \log(r^2 + \epsilon^2) - \frac{\epsilon^2}{r^2 + \epsilon^2} \right), \quad (3.4)$$

$$4\pi\mu u_2 = \frac{f_2 \hat{x}_2^2 + f_1 \hat{x}_1 \hat{x}_2}{r^2 + \epsilon^2} - f_2 \left(\frac{1}{2} \log(r^2 + \epsilon^2) - \frac{\epsilon^2}{r^2 + \epsilon^2} \right). \quad (3.5)$$

The velocity field given by equation (3.4) and (3.5) satisfies the divergence free condition and has no singularity anywhere.

The blob size does affect the numerical result. Fig 3.2 is showing two δ_ϵ functions with $\epsilon = 0.2$ and $\epsilon = 0.5$. Fig 3.3 shows the corresponding G_ϵ and B_ϵ function. Fig 3.4 shows the velocity fields generated by the force $\mathbf{f}_0\delta_\epsilon(\mathbf{x}_0)$ where $\mathbf{f}_0 = (4\pi\mu, 0)$ and $\mathbf{x}_0 = (0, 0)$ with different blob size ($\epsilon = 0.2, \epsilon = 0.5$).

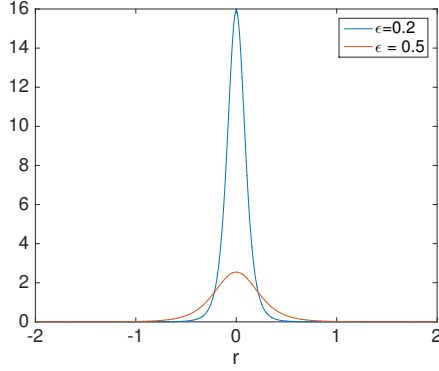


Figure 3.2: Blob function δ_ϵ with $\epsilon = 0.2$ and $\epsilon = 0.5$.

When the velocity is evaluated too far away from where the force is exerted, the Stokes paradox [23] occurs. As seen in (3.2) and (3.3) and their regularized version (3.4) and (3.5), we know that the velocity increases indefinitely with r , which is unphysical. Thus the velocity formula cannot be regarded as valid at points too far away from the forcing point in 2D.

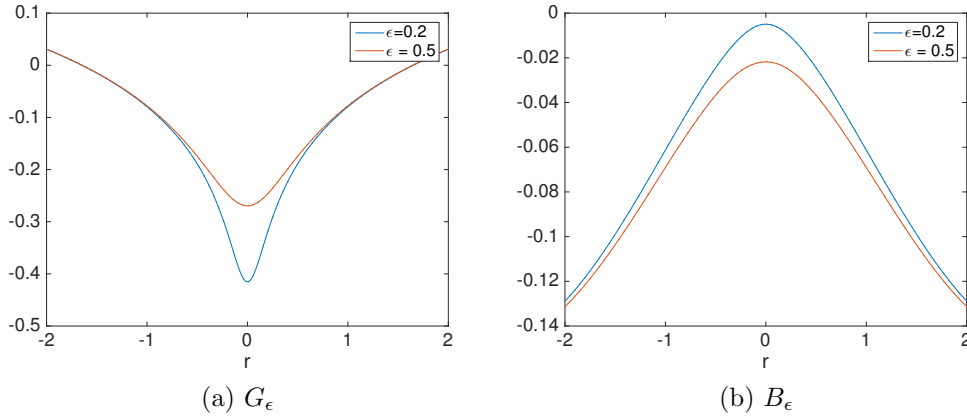


Figure 3.3: B_ϵ and G_ϵ corresponding to $\epsilon = 0.2$ and $\epsilon = 0.5$.

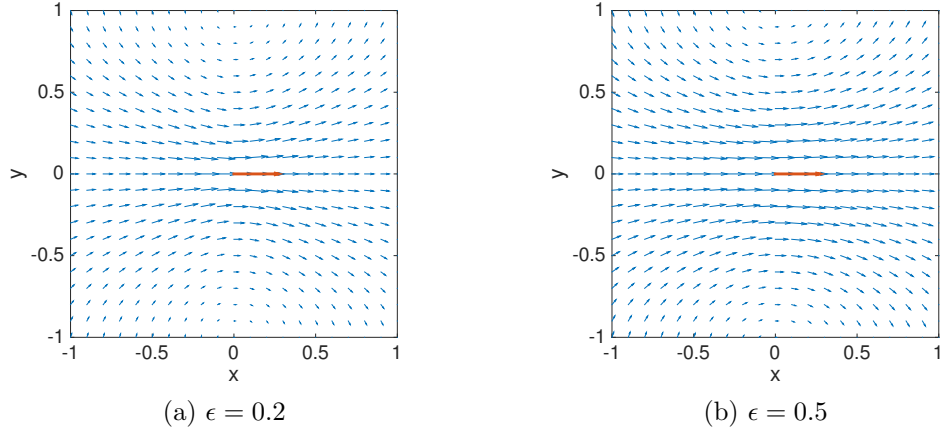


Figure 3.4: Velocity field generated using equation 3.4 and 3.5 by force $\mathbf{f}_0 \delta_\epsilon(\mathbf{x}_0)$ where $\mathbf{f}_0 = (4\pi\mu, 0)$ and $\mathbf{x}_0 = (0, 0)$, with different ϵ ($\epsilon = 0.2$ and $\epsilon = 0.5$). The red arrow shows the direction and magnitude of the force, the the blue arrows are the plotted velocity field.

3.2 Singly Periodic Stokes Case

As shown in Mannan, Cortez [24], we can rewrite the equation for velocity in the free space Stokes case due to a regularized force (f_1, f_2) at (x_1, x_2) , and get

$$\begin{aligned} 4\pi\mu u_1(\mathbf{x}) &= f_1 \left(\frac{\hat{x}_1^2 + \epsilon^2}{r^2 + \epsilon^2} \right) + f_2 \frac{\hat{x}_1 \hat{x}_2}{r^2 + \epsilon^2} - \frac{1}{2} f_1 \log(r^2 + \epsilon^2) \\ &= f_1 - f_1 \frac{\hat{x}_2^2}{r^2 + \epsilon^2} + f_2 \frac{\hat{x}_1 \hat{x}_2}{r^2 + \epsilon^2} - \frac{1}{2} f_1 \log(r^2 + \epsilon^2) \end{aligned} \quad (3.6)$$

$$\begin{aligned} 4\pi\mu u_2(\mathbf{x}) &= f_2 \left(\frac{\hat{x}_2^2 + \epsilon^2}{r^2 + \epsilon^2} \right) + f_1 \frac{\hat{x}_1 \hat{x}_2}{r^2 + \epsilon^2} - \frac{1}{2} f_2 \log(r^2 + \epsilon^2) \\ &= \frac{\hat{x}_2}{r^2 + \epsilon^2} (f_1 \hat{x}_1 + f_2 \hat{x}_2) + f_2 \frac{\epsilon^2}{r^2 + \epsilon^2} - \frac{1}{2} f_2 \log(r^2 + \epsilon^2) \end{aligned} \quad (3.7)$$

Note that

$$\frac{\hat{x}_i \hat{x}_j}{r^2 + \epsilon^2} = \hat{x}_i \frac{\partial}{\partial \hat{x}_j} \left(\frac{1}{2} \log(r^2 + \epsilon^2) \right) \quad (3.8)$$

and

$$\frac{\epsilon^2}{r^2 + \epsilon^2} = \epsilon \frac{\partial}{\partial \epsilon} \left(\frac{1}{2} \log(r^2 + \epsilon^2) \right). \quad (3.9)$$

If we write $\mathcal{G}(r, \epsilon) = \frac{1}{2} \log(r^2 + \epsilon^2)$, then the velocity can be written as

$$4\pi\mu u_1 = f_1 - f_1\mathcal{G}(r, \epsilon) + \hat{x}_2 \left(-f_1 \frac{\partial \mathcal{G}}{\partial \hat{x}_2} + f_2 \frac{\partial \mathcal{G}}{\partial \hat{x}_1} \right)$$

$$4\pi\mu u_2 = \hat{x}_2 \left(f_1 \frac{\partial \mathcal{G}}{\partial \hat{x}_1} + f_2 \frac{\partial \mathcal{G}}{\partial \hat{x}_2} \right) + f_2 \epsilon \frac{\partial \mathcal{G}}{\partial \epsilon} - f_2 \mathcal{G}$$

Now assume periodicity is in x -direction with spatial period of L . The Stokes equations are:

$$0 = -\nabla p + \mu \Delta \mathbf{u} + \sum_{k=-\infty}^{\infty} \mathbf{f}_0 \delta(\mathbf{x} - \mathbf{x}_0 + kL\mathbf{e}_1).$$

Here $\mathbf{e}_1 = (1, 0)$. The regularized singly-periodic Green's function $\mathcal{G}_{\mathcal{P}}$ is

$$\mathcal{G}_{\mathcal{P}}(\hat{x}_1, \hat{x}_2, L, \epsilon) = \sum_{k=-\infty}^{\infty} \frac{1}{2} \log(\epsilon^2 + \hat{x}_2^2 + (\hat{x}_1 + kL)^2). \quad (3.10)$$

Here $(\hat{x}_1, \hat{x}_2) = \mathbf{x} - \mathbf{x}_0$.

Using the identity

$$\sum_{j=-\infty}^{\infty} \log((x + 2\pi j)^2 + \xi^2) = \log(\cosh(\xi) - \cos(x)), \quad (3.11)$$

and the property

$$\lim_{L \rightarrow \infty} \mathcal{G}_{\mathcal{P}}(x_1, x_2, L, \epsilon) = \mathcal{G}(x_1, x_2, \epsilon),$$

we get

$$\mathcal{G}_{\mathcal{P}}(x_1, x_2, L, \epsilon) = \frac{1}{2} \log \left(\cosh \left(\frac{2\pi}{L} \sqrt{x_2^2 + \epsilon^2} \right) - \cos \left(\frac{2\pi x_1}{L} \right) \right) - \frac{1}{2} \log \left(\frac{2\pi^2}{L^2} \right).$$

The velocity equations in the periodic Stokes case are given by equation (3.12) and (3.13)

$$4\pi\mu u_1 = f_1 - f_1\mathcal{G}_{\mathcal{P}}(\hat{x}_1, \hat{x}_2, L, \epsilon) + \hat{x}_2(-f_1\frac{\partial\mathcal{G}_{\mathcal{P}}}{\partial\hat{x}_2} + f_2\frac{\partial\mathcal{G}_{\mathcal{P}}}{\partial\hat{x}_1}) \quad (3.12)$$

$$4\pi\mu u_2 = \hat{x}_2\left(f_1\frac{\partial\mathcal{G}_{\mathcal{P}}}{\partial\hat{x}_1} + f_2\frac{\partial\mathcal{G}_{\mathcal{P}}}{\partial\hat{x}_2}\right) + f_2\epsilon\frac{\partial\mathcal{G}_{\mathcal{P}}}{\partial\epsilon} - f_2\mathcal{G}_{\mathcal{P}} \quad (3.13)$$

Fig 3.5 shows the velocity field in $[-1, 1] \times [-1, 1]$ given a regularized point force $\mathbf{f} = (3\pi\mu, \pi\mu)$ acts on $\mathbf{x}_0 = (0, 0)$ with spatial periodicity of $L = 0.5$ in x -direction. That means the same regularized point force acts on $(-0.5, 0)$, $(0.5, 0)$, $(-1, 0)$, $(1, 0)$, etc.

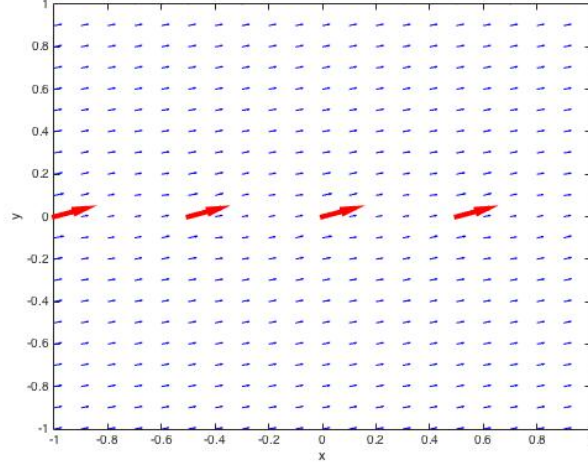


Figure 3.5: Velocity field generated by a point force $(3\pi\mu, \pi\mu)$ acting on the point $(0, 0)$ with spatial periodicity $L = 0.5$ in x -direction.

Fig 3.6 is showing with the choosing of different spatial periodicity, the velocity on y -axis is different. The velocity decays faster as L getting larger.

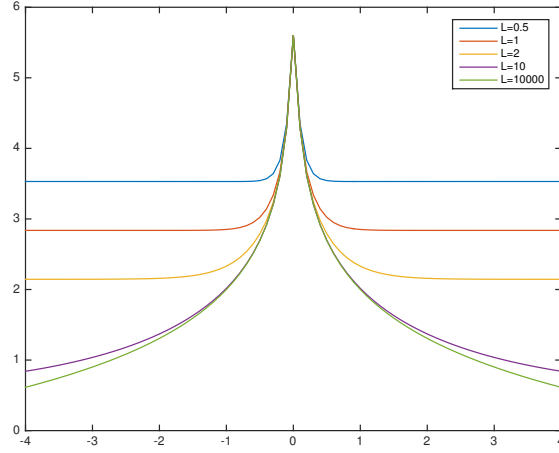


Figure 3.6: Velocity on y -axis generated by a point force $(4\pi\mu, 0)$ acting on $(0, 0)$. Here $\epsilon = 0.01$.

3.3 Oseen Tensor Approximation

3.3.1 Single Oscillator

Here we consider the motion of a spherical object in Stokes fluid using the Oseen tensor. Since our model oscillator moves along the straight line connecting the two trap positions, we only consider the velocity in this direction and study the 1D problem. We assume the moving body in the fluid is a ball with radius a , and the velocity on the surface of the ball is constant. We have the equation of motion:

$$\dot{\hat{x}} = \frac{1}{8\pi\mu}(1 - 2\log(a))F$$

in 2D and

$$\dot{\hat{x}} = \frac{1}{6\pi\mu a}F$$

in 3D respectively where the force F exerted on the centroid of the ball. The harmonic potential gives the driven force of oscillation:

$$F = \kappa(\tilde{x} - \hat{x}).$$

Here κ is the trapping stiffness and \hat{x} , \tilde{x} are the centroid position of moving body and active trap respectively.

By considering the relative position of the oscillator from the active trap, we define

$$x = \hat{x} - \tilde{x}$$

and get

$$\dot{x} = Ax$$

where $A = -\frac{\kappa(1 - 2\log(a))}{8\pi\mu}$ in 2D and $A = -\frac{\kappa}{6\pi\mu a}$ in 3D.

That is

$$x(t) = \exp(At)x(0)$$

To compute the temporal period, we compute the time required for the oscillator to move from initial position $x(0) = \lambda - \xi$, where the oscillator is farthest away from the active trap, to the position at which trap switches at $x(T) = \xi$. The full temporal period is $P = 2T$. A figure to illustrate the start and end position of the oscillator and trap for the computed time is shown in Fig 3.7.

Plug in $x(0) = \lambda - \xi$ and $x(T) = \xi$ to the equation above, we get

$$\begin{aligned}\xi &= \exp(AT)(\lambda - \xi) \\ AT &= \log\left(\frac{\xi}{\lambda - \xi}\right) \\ T &= -\frac{1}{A} \log\left(\frac{\lambda}{\xi} - 1\right)\end{aligned}$$

Thus, the temporal period for a single oscillator is

$$P = \frac{16\pi\mu}{\kappa(1 - 2\log(a))} \log\left(\frac{\lambda}{\xi} - 1\right)$$

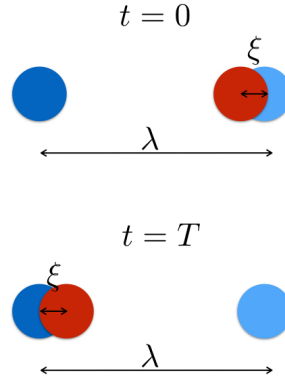


Figure 3.7: The initial and end figure for the computed period. Blue circle is the active trap, the light blue one is the inactive trap, and the red one is the oscillator. At $t = 0$, the oscillator is farthest away from the trap and moving left, it switches moving direction at $t = T$, when the threshold distance ξ is reached.

in $2D$ and

$$P = \frac{12\pi\mu a}{\kappa} \log\left(\frac{\lambda}{\xi} - 1\right)$$

in $3D$.

3.3.2 Two Oscillators

For the coupling of two oscillators placed next to each other, we could also use Oseen tensor to study the coupling state. We assume two oscillators are placed on x -axis with the centroid position $(\hat{x}_1(t), 0)$ and $(\hat{x}_2(t), 0)$, and the corresponding acting traps are at the position $(\tilde{x}_1, 0)$ and $(\tilde{x}_2, 0)$. The external forces acting on two oscillators are expressed as

$$f_1 = \kappa(\tilde{x}_1 - \hat{x}_1)$$

and

$$f_2 = \kappa(\tilde{x}_2 - \hat{x}_2)$$

in x -direction respectively, and 0 in y -direction. Here κ is the trapping spring stiffness between the trap and the immersed body.

1. 2D case

For the 2D case, the velocity in y -direction for both oscillators are zero, and the velocity of two forces acting on two oscillators in x -direction are:

(a) The effect of f_1 on \hat{x}_1 :

$$8\pi\mu u(\hat{x}_1) = \kappa(\tilde{x}_1 - \hat{x}_1)(1 - 2\log a)$$

(b) The effect of f_1 on \hat{x}_2 :

$$4\pi\mu u(\hat{x}_2) = \kappa(\tilde{x}_1 - \hat{x}_1)(1 - \log(|\hat{x}_1 - \hat{x}_2|))$$

(c) The effect of f_2 on \hat{x}_1 :

$$4\pi\mu u(\hat{x}_1) = \kappa(\tilde{x}_2 - \hat{x}_2)(1 - \log|\hat{x}_1 - \hat{x}_2|)$$

(d) The effect of f_2 on \hat{x}_2 :

$$8\pi\mu u(\hat{x}_2) = \kappa(\tilde{x}_2 - \hat{x}_2)(1 - 2\log a)$$

Based on the linearity of the Stokes equations, we have

$$8\pi\mu\dot{\hat{x}}_1 = \kappa((\tilde{x}_1 - \hat{x}_1)(1 - 2\log a) + 2(\tilde{x}_2 - \hat{x}_2)(1 - \log(|\hat{x}_1 - \hat{x}_2|)))$$

$$8\pi\mu\dot{\hat{x}}_2 = \kappa((\tilde{x}_2 - \hat{x}_2)(1 - 2\log a) + (\tilde{x}_1 - \hat{x}_1)(1 - \log(|\hat{x}_1 - \hat{x}_2|)))$$

By using $x_i = \tilde{x}_i - \hat{x}_i$ which is the relative position of the oscillator to the active trap, and approximate $|\hat{x}_1 - \hat{x}_2|$ by the distance between two oscillators d , we have

$$\begin{aligned} 8\pi\mu\dot{x}_1 &= -\kappa(x_1(1 - 2\log a) + 2x_2(1 - \log d)) \\ 8\pi\mu\dot{x}_2 &= -\kappa(x_2(1 - 2\log a) + 2x_1(1 - \log d)) \end{aligned}$$

Here $\dot{x}_i = u(x_i) = \frac{dx_i}{dt}$ for $i = 1, 2$.

We can use change of variable $x_1 = \tilde{x}_1 - \hat{x}_1$ and $x_2 = \tilde{x}_2 - \hat{x}_2$, which is the relative position of the immersed body to the corresponding acting trap. Let $x_{\pm} = x_1 \pm x_2$, we get

$$\begin{aligned} \dot{x}_+ &= -\frac{\kappa}{8\pi\mu}x_+(3 - 2\log a - 2\log d) \\ \dot{x}_- &= -\frac{\kappa}{8\pi\mu}x_-(2\log d - 2\log a - 1) \end{aligned}$$

$x_+ = 0$ (anti-phase) and $x_- = 0$ (in-phase) are equilibrium solutions.

2. 3D Case

For the 3D case discussed in [4], we use the same notation, and get

$$\begin{aligned} \dot{x}_1 &= -\frac{\kappa}{\gamma} \left(x_1 + \frac{3a}{2d}x_2 \right) \\ \dot{x}_2 &= -\frac{\kappa}{\gamma} \left(x_2 + \frac{3a}{2d}x_1 \right) \end{aligned}$$

here $\gamma = 6\pi\mu a$.

Similar to the 2D case,

$$\dot{x}_{\pm} = -\frac{\kappa}{\gamma}x_{\pm} \left(1 \pm \frac{3a}{2d}\right) \quad (3.14)$$

$$x_{\pm}(t) = x_{\pm}(0) \exp \left(-\frac{\kappa}{\gamma}t \left(1 \pm \frac{3a}{2d}\right) \right) \quad (3.15)$$

This shows that exact in-phase and exact anti-phase are equilibrium states.

Also, both are stable if the switching of trap positions does not occur.

From (3.15), we have

$$\begin{aligned} 2x_1(t) &= (x_1(0) + x_2(0)) A(t) + (x_1(0) - x_2(0)) B(t) \\ &= x_1(0)(A(t) + B(t)) + x_2(0)(A(t) - B(t)) \end{aligned} \quad (3.16)$$

$$\begin{aligned} 2x_2(t) &= (x_1(0) + x_2(0)) A(t) - (x_1(0) - x_2(0)) B(t) \\ &= x_1(0)(A(t) - B(t)) + x_2(0)(A(t) + B(t)) \end{aligned} \quad (3.17)$$

Here $A(t)$ and $B(t)$ are defined as

$$\begin{aligned} A(t) &= \exp \left(-\frac{k}{\gamma}(1 + \sigma)t \right) \\ B(t) &= \exp \left(-\frac{k}{\gamma}(1 - \sigma)t \right) \end{aligned}$$

$\sigma = \frac{3a}{2d}$ is a small constant.

We have two equilibrium state: in-phase and anti-phase. Now we take trap switching into consideration and analytically study the stability of two states.

(a) Anti-phase State

For the anti-phase case, we assume two oscillators start at $x_1(0) = -\eta = -(\lambda - \xi)$, $x_2(0) = \eta(1 - h)$. Here h is a perturbation parameter of $\mathcal{O}(\sigma)$. We indicate the time when the second immersed body (IB2) switches direction

as t_1 . If $h \neq 0$, the first immersed body (IB1) will be close to the switching point, but not there yet. At $t_2 > t_1$, IB1 reaches the switching point and IB2 moved to a new position $x_2(t_2)$. We can get the new perturbation as

$$x_2(t_2) = -\eta(1 - h_{new}) \quad (3.18)$$

If $h_{new} < h$, we know the perturbation is decreasing so the anti-phase configuration stable.

We summarize the relative position of the two oscillators in Table 3.1. An illustration graph showing the positions of the oscillators and traps at the critical time is shown in Fig 3.8.

time	$x_1(t)$	$x_2(t)$
0	$-\eta$	$\eta(1 - h)$
t_1 (before IB2 switches trap)	$x_1(t_1)$	ξ
t_1 (after IB2 switches trap)	$x_1(t_1)$	$-\eta$
t_2	$-\xi$	$x_2(t_2)$

Table 3.1: Relative position of two immersed bodies in critical times for anti-phase state.

From (3.16) and (3.17), we have

$$2x_1(t_1) = -\eta h A(t_1) - \eta(2 - h)B(t_1) \quad (3.19)$$

$$2\xi = -\eta h A(t_1) + \eta(2 - h)B(t_1) \quad (3.20)$$

$$-2\xi = x_1(t_1)(A(t_2 - t_1) + B(t_2 - t_1)) - \eta(A(t_2 - t_1) - B(t_2 - t_1)) \quad (3.21)$$

$$2x_2(t_2) = x_1(t_1)(A(t_2 - t_1) - B(t_2 - t_1)) - \eta(A(t_2 - t_1) + B(t_2 - t_1)) \quad (3.22)$$

If IB1 and IB2 are in exact anti-phase state, then $h = 0$. In that case, by

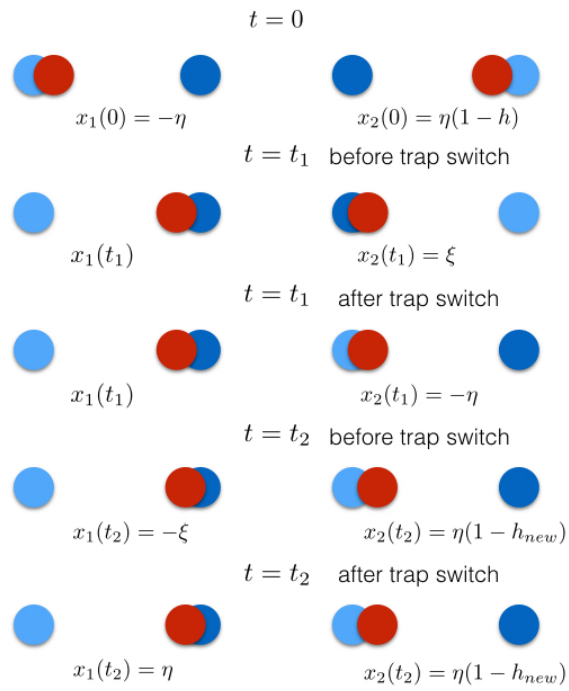


Figure 3.8: Relative position of the oscillators at the critical times, perturbed anti-phase case.

(3.20), we have

$$\begin{aligned}
2\xi &= 2\eta B(t_1) \\
\frac{\xi}{\eta} &= B(t_1) \\
t_1 &= \frac{\gamma}{\kappa} \frac{1}{1-\sigma} C \\
&= \frac{\gamma}{\kappa} (1 + \sigma + \sigma^2) C + \mathcal{O}(\sigma^3)
\end{aligned}$$

Here $C = \log\left(\frac{\eta}{\xi}\right)$ is a positive constant.

If IB1 and IB2 are not exactly anti-phase, we would have $h \neq 0$ and we can assume

$$t_1 = a_0 + a_1 h + a_2 h^2 + \mathcal{O}(h^3)$$

Here $a_0 = \frac{\gamma}{\kappa} (1 + \sigma + \sigma^2) C$, and $h = \mathcal{O}(\sigma)$.

Then we can write

$$\begin{aligned}
A(t_1) &= \exp\left(-\frac{\kappa}{\gamma}(1+\sigma)\left(\frac{\gamma}{\kappa}C(1+\sigma+\sigma^2) + a_1 h + a_2 h^2 + \mathcal{O}(h^3)\right)\right) \\
&= \exp\left(-C - 2\sigma C(1+\sigma) - \frac{\kappa}{\gamma}h(a_1 + a_1\sigma + a_2 h) + \mathcal{O}(h^3)\right) \\
&= \frac{\xi}{\eta}\left(1 - 2C\sigma - \frac{\kappa}{\gamma}a_1 h + 2C(-1+C)\sigma^2 + \frac{\kappa}{\gamma}a_1(-1+2C)h\sigma\right. \\
&\quad \left.+ \left(-\frac{\kappa}{\gamma}a_2 + \frac{1}{2}\frac{\kappa^2}{\gamma^2}a_1^2\right)h^2\right) + \mathcal{O}(h^3)
\end{aligned}$$

$$\begin{aligned}
-\eta h A(t_1) &= -\eta h \frac{\xi}{\eta}\left(1 - 2C\sigma - \frac{\kappa}{\gamma}a_1 h + 2C(-1+C)\sigma^2 + \right. \\
&\quad \left. \frac{\kappa}{\gamma}a_1(-1+2C)h\sigma + \left(-\frac{\kappa}{\gamma}a_2 + \frac{1}{2}\frac{\kappa^2}{\gamma^2}a_1^2\right)h^2\right) + \mathcal{O}(h^3) \quad (3.23) \\
&= \xi\left(-h + 2Ch\sigma + \frac{\kappa}{\gamma}a_1 h^2\right) + \mathcal{O}(h^3)
\end{aligned}$$

$$\begin{aligned}
B(t_1) &= \exp \left(-\frac{\kappa}{\gamma}(1-\sigma) \left(\frac{\gamma}{\kappa}C(1+\sigma+\sigma^2) + a_1h + a_2h^2 + \mathcal{O}(\sigma^3) \right) \right) \\
&= \exp \left(-C - \frac{\kappa}{\gamma}h(a_1 - a_1\sigma + a_2h) + \mathcal{O}(\sigma^3) \right) \\
&= \frac{\xi}{\eta} \left(1 - \frac{\kappa}{\gamma}a_1h + \frac{\kappa}{\gamma}a_1h\sigma + \left(-\frac{\kappa}{\gamma}a_2 + \frac{1}{2}\frac{\kappa^2}{\gamma^2}a_1^2 \right) h^2 \right) + \mathcal{O}(\sigma^3)
\end{aligned}$$

$$\begin{aligned}
\eta(2-h)B(t_1) &= \eta(2-h) \frac{\xi}{\eta} \left(1 - \frac{\kappa}{\gamma}a_1h + \frac{\kappa}{\gamma}a_1h\sigma + \left(-\frac{\kappa}{\gamma}a_2 + \frac{1}{2}\frac{\kappa^2}{\gamma^2}a_1^2 \right) h^2 \right) \\
&\quad + \mathcal{O}(\sigma^3) \\
&= \xi \left(2 - \left(1 + 2\frac{\kappa}{\gamma}a_1 \right) h + 2\frac{\kappa}{\gamma}a_1h\sigma + \right. \\
&\quad \left. \left(\frac{\kappa}{\gamma}a_1 - 2\frac{\kappa}{\gamma}a_2 + \frac{\kappa^2}{\gamma^2}a_1^2 \right) h^2 \right) + \mathcal{O}(\sigma^3)
\end{aligned} \tag{3.24}$$

By combining (3.20), (3.23) and (3.24), we have

$$\begin{aligned}
2 &= 2 - \left(2 + 2\frac{\kappa}{\gamma}a_1 \right) h + 2 \left(C + \frac{\kappa}{\gamma}a_1 \right) h\sigma + \\
&\quad \left(2\frac{\kappa}{\gamma}a_1 - 2\frac{\kappa}{\gamma}a_2 + \frac{\kappa^2}{\gamma^2}a_1^2 \right) h^2 + \mathcal{O}(\sigma^3)
\end{aligned}$$

That means

$$\begin{aligned}
1 + \frac{\kappa}{\gamma}a_1 &= 0 \\
\left(C + \frac{\kappa}{\gamma}a_1 \right) h\sigma + \left(\frac{\kappa}{\gamma}a_1 - \frac{\kappa}{\gamma}a_2 + \frac{1}{2}\frac{\kappa^2}{\gamma^2}a_1^2 \right) h^2 &= 0
\end{aligned}$$

We can get

$$\begin{aligned} a_1 &= -\frac{\gamma}{\kappa} \\ a_2 &= \frac{\gamma}{\kappa} \left((C-1)\frac{\sigma}{h} - \frac{1}{2} \right). \end{aligned}$$

By plugging in the value of a_1 and a_2 into (3.19), we have

$$x_1(t_1) = -\xi (1 + h - 2Ch\sigma + h^2) + \mathcal{O}(\sigma^3).$$

Now we consider the time period from t_1 to t_2 . When the $h = 0$, two oscillators are in exact anti-phase and $t_2 - t_1 = 0$. In the perturbed case, we assume

$$t_2 - t_1 = b_1 h + b_2 h^2 + \mathcal{O}(\sigma^3)$$

Then

$$\begin{aligned} A(t_2 - t_1) &= \exp \left(-\frac{\kappa}{\gamma} (1 + \sigma) (b_1 h + b_2 h^2) + \mathcal{O}(\sigma^3) \right) \\ &= \exp \left(-\frac{\kappa}{\gamma} h (b_1 + b_1 \sigma + b_2 h) + \mathcal{O}(\sigma^3) \right) \\ &= 1 - \frac{\kappa}{\gamma} b_1 h - \frac{\kappa}{\gamma} b_1 h \sigma + \left(-\frac{\kappa}{\gamma} b_2 + \frac{1}{2} \frac{\kappa^2}{\gamma^2} b_1^2 \right) h^2 + \mathcal{O}(\sigma^3) \end{aligned}$$

$$\begin{aligned} B(t_2 - t_1) &= \exp \left(-\frac{\kappa}{\gamma} (1 - \sigma) (b_1 h + b_2 h^2) + \mathcal{O}(\sigma^3) \right) \\ &= \exp \left(-\frac{\kappa}{\gamma} h (b_1 - b_1 \sigma + b_2 h) + \mathcal{O}(\sigma^3) \right) \\ &= 1 - \frac{\kappa}{\gamma} b_1 h + \frac{\kappa}{\gamma} b_1 h \sigma + \left(-\frac{\kappa}{\gamma} b_2 + \frac{1}{2} \frac{\kappa^2}{\gamma^2} b_1^2 \right) h^2 + \mathcal{O}(\sigma^3) \end{aligned}$$

$$\begin{aligned}
A(t_2 - t_1) + B(t_2 - t_1) &= 2 \left(1 - \frac{\kappa}{\gamma} b_1 h + \left(-\frac{\kappa}{\gamma} b_2 + \frac{1}{2} \frac{\kappa^2}{\gamma^2} b_1^2 \right) h^2 \right) + \\
&\quad \mathcal{O}(\sigma^3) \\
A(t_2 - t_1) - B(t_2 - t_1) &= -2 \frac{\kappa}{\gamma} b_1 h \sigma + \mathcal{O}(\sigma^3)
\end{aligned}$$

By (3.21), we know

$$\begin{aligned}
-2\xi &= -2\xi(1 + h - 2Ch\sigma + h^2) \left(1 - \frac{\kappa}{\gamma} b_1 h + \right. \\
&\quad \left. \left(-\frac{\kappa}{\gamma} b_2 + \frac{1}{2} \frac{\kappa^2}{\gamma^2} b_1^2 \right) h^2 \right) + 2\eta \frac{\kappa}{\gamma} b_1 h \sigma + \mathcal{O}(\sigma^3) \\
&= -2\xi \left(1 + \left(1 - \frac{\kappa}{\gamma} b_1 \right) h - 2Ch\sigma + \right. \\
&\quad \left. \left(1 - \frac{\kappa}{\gamma} b_1 - \frac{\kappa}{\gamma} b_2 + \frac{1}{2} \frac{\kappa^2}{\gamma^2} b_1^2 \right) h^2 \right) + 2\eta \frac{\kappa}{\gamma} b_1 h \sigma + \mathcal{O}(\sigma^3)
\end{aligned}$$

That gives us

$$\begin{aligned}
b_1 &= \frac{\gamma}{\kappa} \\
b_2 &= \frac{\gamma}{\kappa} \left(\frac{1}{2} - \frac{\sigma}{h} \left(2C + \frac{\eta}{\xi} \right) \right).
\end{aligned}$$

Plugging in the values of b_1 and b_2 into (3.22), we have

$$\begin{aligned}
2x_2(t_2) &= x_1(t_1)(A - B)(t_2 - t_1) + x_2(t_1)(A + B)(t_2 - t_1) \\
&= -\xi(1 + h - 2Ch\sigma) \left(-2 \frac{\kappa}{\gamma} b_1 h \sigma \right) \\
&\quad - 2\eta \left(1 - \frac{\kappa}{\gamma} b_1 h + \left(-\frac{\kappa}{\gamma} b_2 + \frac{1}{2} \frac{\kappa^2}{\gamma^2} b_1^2 \right) h^2 \right) + \mathcal{O}(\sigma^3) \\
&= 2\xi h \sigma - 2\eta \left(1 - h + \left(2C + \frac{\eta}{\xi} \right) h \sigma \right) + \mathcal{O}(\sigma^3)
\end{aligned}$$

$$x_2(t_2) = -\eta \left(1 - h + \left(2C + \frac{\eta}{\xi} - \frac{\xi}{\eta} \right) h\sigma \right) + \mathcal{O}(\sigma^3) \quad (3.25)$$

We have

$$h_{new} = h \left(1 - \sigma \left(\frac{\eta^2 - \xi^2}{\eta\xi} + 2 \log \left(\frac{\eta}{\xi} \right) \right) \right)$$

Since $\eta = \lambda - \xi > \xi$ and σ is small, we know

$$h_{new} < h$$

That means for the perturbed anti-phase case, the perturbation is decreasing, thus anti-phase state is stable.

(b) In-phase State

For the in-phase case, we assume the two oscillators start at $x_1(0) = \eta$, $x_2(0) = \eta(1 - h)$, where h is the initial perturbation as defined in the anti-phase above, and h is $\mathcal{O}(\sigma)$. The time at which IB2 switches is t_1 . If IB1 and IB2 are exactly in-phase, then IB1 and IB2 switch direction at the same time. If not, there are two possible things that can happen: active trap related to oscillator 1 switches position first, or active trap related to oscillator 2 switches position first. We denote the first possibility as case (1), and the second one as case (2). We study both cases to see if they could happen, and also do the stability study. The relative positions of the two immersed bodies are summarized in Table 3.2. The illustration figure showing the position of traps and oscillators at critical time with both possibility is shown in Fig 3.9.

From (3.16) and (3.17), we have

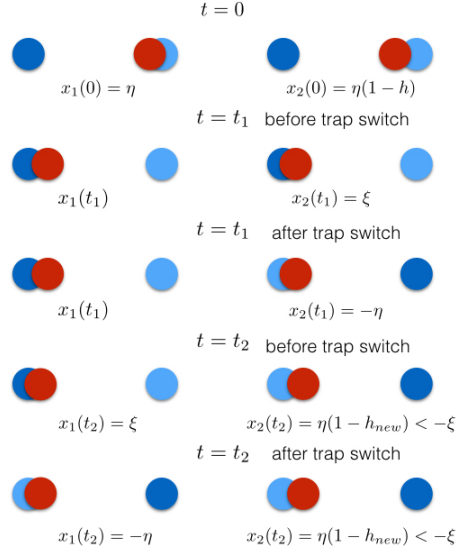
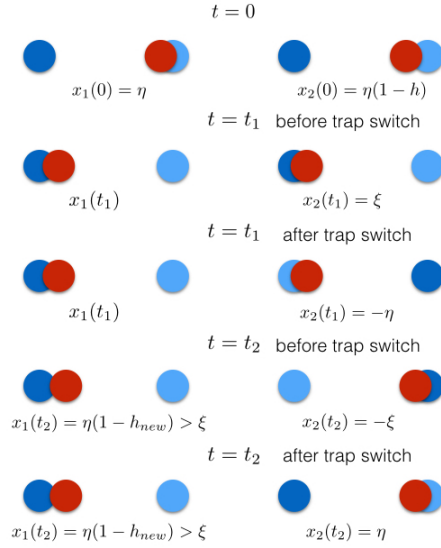
(a) Case (1), x_1 switches direction first.(b) Case (2), x_2 switches direction first.

Figure 3.9: Relative position of the oscillators at the critical times, perturbed in-phase case.

time	$x_1(t)$	$x_2(t)$
0	η	$\eta(1-h)$
t_1 (before IB2 switches trap)	$x_1(t_1)$	ξ
t_1 (after IB2 switches trap)	$x_1(t_1)$	$-\eta$
t_2 (if case(1) happens)	ξ	$x_2(t_2) (< -\xi)$
t_2 (if case(2) happens)	$x_1(t_2) (> \xi)$	$-\xi$

Table 3.2: Relative position of two immersed bodies in critical times for in-phase state.

$$2x_1(t_1) = \eta(2-h)A(t_1) + \eta h B(t_1) \quad (3.26)$$

$$2\xi = \eta(2-h)A(t_1) - \eta h B(t_1) \quad (3.27)$$

If IB1 and IB2 are exact in-phase, we have $h = 0$. From (3.27), we have

$$\begin{aligned}
2\xi &= 2\eta A(t_1) \\
\frac{\xi}{\eta} &= A(t_1) \\
t_1 &= \frac{\gamma}{\kappa} \frac{1}{1+\sigma} C \\
&= \frac{\gamma}{\kappa} (1 - \sigma + \sigma^2) C + \mathcal{O}(\sigma^3)
\end{aligned}$$

If IB1 and IB2 are not exact in-phase, we assume

$$t_1 = c_0 + c_1 h + c_2 h^2 + \mathcal{O}(\sigma^3)$$

Here $c_0 = \frac{\gamma}{\kappa} (1 - \sigma + \sigma^2) C$.

$$\begin{aligned}
A(t_1) &= \exp \left(-\frac{\kappa}{\gamma}(1+\sigma) \left(\frac{\gamma}{\kappa}(1-\sigma+\sigma^2)C + c_1h + c_2h^2 \right) + \mathcal{O}(\sigma^3) \right) \\
&= \exp \left(-C - \frac{\kappa}{\gamma}h(c_1 + c_1\sigma + c_2h) + \mathcal{O}(\sigma^3) \right) \\
&= \frac{\xi}{\eta} \left(1 - \frac{\kappa}{\gamma}c_1h - \frac{\kappa}{\gamma}c_1h\sigma + \left(-\frac{\kappa}{\gamma}c_2 + \frac{1}{2}\frac{\kappa^2}{\gamma^2}c_1^2 \right) h^2 \right) + \mathcal{O}(\sigma^3)
\end{aligned}$$

$$\begin{aligned}
\eta(2-h)A(t_1) &= \eta(2-h) \frac{\xi}{\eta} \left(1 - \frac{\kappa}{\gamma}c_1h - \frac{\kappa}{\gamma}c_1h\sigma + \left(-\frac{\kappa}{\gamma}c_2 + \frac{1}{2}\frac{\kappa^2}{\gamma^2}c_1^2 \right) h^2 \right) \\
&\quad + \mathcal{O}(\sigma^3) \\
&= \xi \left(2 - \left(1 + 2\frac{\kappa}{\gamma}c_1 \right) h - 2\frac{\kappa}{\gamma}c_1h\sigma + \frac{\kappa}{\gamma} \left(c_1 - 2c_2 + \frac{\kappa}{\gamma}c_1^2 \right) h^2 \right) \\
&\quad + \mathcal{O}(\sigma^3)
\end{aligned} \tag{3.28}$$

$$\begin{aligned}
B(t_1) &= \exp \left(-\frac{\kappa}{\gamma}(1-\sigma) \left(\frac{\gamma}{\kappa}(1-\sigma+\sigma^2)C + c_1h + c_2h^2 \right) + \mathcal{O}(\sigma^3) \right) \\
&= \exp \left(-C + 2C\sigma(1-\sigma) - \frac{\kappa}{\gamma}h(c_1 - c_1\sigma + c_2h) + \mathcal{O}(\sigma^3) \right) \\
&= \frac{\xi}{\eta} \left(1 + 2C\sigma - \frac{\kappa}{\gamma}hc_1 \right) + \mathcal{O}(\sigma^2)
\end{aligned}$$

$$-\eta hB(t_1) = \xi \left(-h - 2Ch\sigma + \frac{\kappa}{\gamma}c_1h^2 \right) + \mathcal{O}(\sigma^3) \tag{3.29}$$

By combining (3.27), (3.28), (3.29), we have

$$2 = 2 - \left(2 + 2\frac{\kappa}{\gamma}c_1 \right) h - 2 \left(\frac{\kappa}{\gamma}c_1 + C \right) h\sigma + \frac{\kappa}{\gamma} \left(2c_1 - 2c_2 + \frac{\kappa}{\gamma}c_1^2 \right) h^2 + \mathcal{O}(\sigma^3)$$

That means

$$c_1 = -\frac{\gamma}{\kappa}$$

$$c_2 = \frac{\gamma}{\kappa} \left((1 - C) \frac{\sigma}{h} - \frac{1}{2} \right)$$

By plugging in the value of c_1 and c_2 into (3.26), we have

$$x_1(t_1) = \xi(1 + h + 2Ch\sigma + h^2) + \mathcal{O}(\sigma^3)$$

Now we consider the time period from t_1 to t_2 . We assume

$$t_2 - t_1 = d_0 + d_1h + d_2h^2 + \mathcal{O}(\sigma^3)$$

Then

$$\begin{aligned} A(t_2 - t_1) &= \exp \left(-\frac{\kappa}{\gamma} (1 + \sigma)(d_0 + d_1h + d_2h^2) + \mathcal{O}(\sigma^3) \right) \\ &= \exp \left(-\frac{\kappa}{\gamma} (d_0 + d_0\sigma + d_1h + d_1h\sigma + d_2h^2) + \mathcal{O}(\sigma^3) \right) \\ &= D \left(1 - \frac{\kappa}{\gamma} d_0\sigma - \frac{\kappa}{\gamma} d_1h + \frac{1}{2} \frac{\kappa^2}{\gamma^2} d_0^2 \sigma^2 + \left(-\frac{\kappa}{\gamma} d_1 + \frac{\kappa^2}{\gamma^2} d_0 d_1 \right) h\sigma \right. \\ &\quad \left. + \left(-\frac{\kappa}{\gamma} d_2 + \frac{1}{2} \frac{\kappa^2}{\gamma^2} d_1^2 \right) h^2 \right) + \mathcal{O}(\sigma^3) \end{aligned}$$

$$\begin{aligned} B(t_2 - t_1) &= \exp \left(-\frac{\kappa}{\gamma} (1 - \sigma)(d_0 + d_1h + d_2h^2) + \mathcal{O}(\sigma^3) \right) \\ &= \exp \left(-\frac{\kappa}{\gamma} (d_0 - d_0\sigma + d_1h - d_1h\sigma + d_2h^2) + \mathcal{O}(\sigma^3) \right) \\ &= D \left(1 + \frac{\kappa}{\gamma} d_0\sigma - \frac{\kappa}{\gamma} d_1h + \frac{1}{2} \frac{\kappa^2}{\gamma^2} d_0^2 \sigma^2 + \left(\frac{\kappa}{\gamma} d_1 - \frac{\kappa^2}{\gamma^2} d_0 d_1 \right) h\sigma \right. \\ &\quad \left. + \left(-\frac{\kappa}{\gamma} d_2 + \frac{1}{2} \frac{\kappa^2}{\gamma^2} d_1^2 \right) h^2 \right) + \mathcal{O}(\sigma^3) \end{aligned}$$

$$\begin{aligned}
(A+B)(t_2-t_1) &= 2D \left(1 - \frac{\kappa}{\gamma} (d_1 h + d_2 h^2) + \frac{1}{2} \frac{\kappa^2}{\gamma^2} (d_0^2 \sigma^2 + d_1^2 h^2) \right) + \mathcal{O}(\sigma^3) \\
(A-B)(t_2-t_1) &= 2D \left(-\frac{\kappa}{\gamma} d_0 \sigma - \frac{\kappa}{\gamma} d_1 h \sigma + \frac{\kappa^2}{\gamma^2} d_0 d_1 h \sigma \right) + \mathcal{O}(\sigma^3)
\end{aligned}$$

Here $D = \exp\left(-\frac{\kappa}{\gamma} d_0\right)$.

If Case(1) happens,

$$2\xi = x_1(t_1)(A(t_2-t_1) + B(t_2-t_1)) - \eta(A(t_2-t_1) - B(t_2-t_1)) \quad (3.30)$$

$$2x_2(t_2) = x_1(t_1)(A(t_2-t_1) - B(t_2-t_1)) - \eta(A(t_2-t_1) + B(t_2-t_1)) \quad (3.31)$$

By (3.30),

$$\begin{aligned}
2\xi &= 2\xi D(1 + h + 2Ch + h^2) \left(1 - \frac{k}{\gamma} d_0 h - \frac{k}{\gamma} d_2 h^2 + \frac{1}{2} \frac{k^2}{\gamma^2} d_0^2 \sigma^2 + \frac{1}{2} \frac{k^2}{\gamma^2} d_1^2 h^2 \right) \\
&\quad + 2\eta D \left(\frac{k}{\gamma} d_0 \sigma + \frac{k}{\gamma} d_1 h \sigma - \frac{k^2}{\gamma^2} d_0 d_1 h \sigma \right) + \mathcal{O}(\sigma^3)
\end{aligned}$$

That gives us

$$D = 1$$

$$d_0 = 0$$

$$d_1 = \frac{\gamma}{\kappa}$$

$$d_2 = \frac{\gamma}{\kappa} \left(\frac{1}{2} + \frac{\sigma}{h} \left(2C + \frac{\eta}{\xi} \right) \right)$$

By plugging in the values of d_0, d_1, d_2 into (3.31), we have

$$\begin{aligned}
2x_2(t_2) &= 2\xi(1 + h + 2Ch + h^2)(-h\sigma) - 2\eta(1 - h - \frac{\kappa}{\gamma}d_2h^2 + \frac{1}{2}h^2) + \mathcal{O}(\sigma^3) \\
&= -2\eta\left(1 - h - \left(2C + \frac{\eta}{\xi} - \frac{\xi}{\eta}\right)h\epsilon\right) + \mathcal{O}(\epsilon^3) \\
x_2(t_2) &= -\eta\left(1 - h - \left(2C + \frac{\eta}{\xi} - \frac{\xi}{\eta}\right)h\sigma\right) + \mathcal{O}(\sigma^3)
\end{aligned}$$

If we define h_{new} as in the anti-phase case, we have

$$h_{new} = h\left(1 + \left(\frac{\eta}{\xi} - \frac{\xi}{\eta} + 2\log\left(\frac{\eta}{\xi}\right)\right)\sigma\right) > h.$$

This means the perturbation increases in the in-phase case, so the in-phase state is unstable if we have Case 1.

If Case (2) happens,

$$2x_1(t_2) = x_1(t_1)(A(t_2 - t_1) + B(t_2 - t_1)) - \eta(A(t_2 - t_1) - B(t_2 - t_1)) \quad (3.32)$$

$$-2\xi = x_1(t_1)(A(t_2 - t_1) - B(t_2 - t_1)) - \eta(A(t_2 - t_1) + B(t_2 - t_1)) \quad (3.33)$$

By (3.33),

$$\begin{aligned}
-2\xi &= 2\xi D(1 + h + 2Ch\sigma + h^2)\left(-\frac{\kappa}{\gamma}d_0\sigma - \frac{\kappa}{\gamma}d_1h\sigma + \frac{\kappa^2}{\gamma^2}d_0d_1h\sigma\right) \\
&\quad - 2\eta D\left(1 - \frac{\kappa}{\gamma}d_1h - \frac{\kappa}{\gamma}d_2h^2 + \frac{1}{2}\frac{\kappa^2}{\gamma^2}d_0^2\sigma^2 + \frac{1}{2}\frac{\kappa^2}{\gamma^2}d_1^2h^2\right) + \mathcal{O}(\sigma^3) \\
&= -2\eta D - 2\eta D\frac{\kappa}{\gamma}d_0h + 2\xi D\frac{\kappa}{\gamma}d_0\sigma + \mathcal{O}(\sigma^2)
\end{aligned}$$

That means

$$\begin{aligned}\xi &= \eta D \\ 2\eta D \frac{\kappa}{\gamma} d_1 h - 2\xi D \frac{\kappa}{\gamma} d_0 \sigma &= 0\end{aligned}$$

Which means $D = \xi/\eta$.

By plugging D in (3.32), we have

$$\begin{aligned}2x_1(t_2) &= 2\xi D + \mathcal{O}(\epsilon) \\ x_1(t_2) &= \xi \frac{\xi}{\eta} < \xi\end{aligned}$$

This contradicts to the assumption that $x_1(t_2) > \xi$ for case 2, thus case 2 will not happen.

Chapter 4

Numerical Simulation of Stokes Case

4.1 Numerical Method

We use the method of regularized Stokeslets introduced in [22] to perform numerical simulations of oscillators in a zero Reynolds number flow. An illustration showing the parameters used in the model is shown in Fig 4.1.

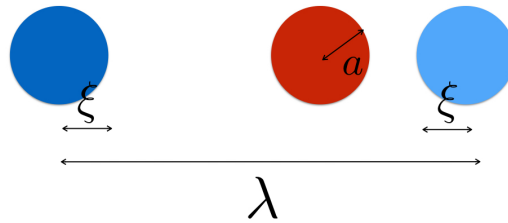


Figure 4.1: Illustration graph for single oscillator system.

We use the explicit solution for the velocity due to a collection of regularized forces. Our procedure is as follows:

1. Set up the values of parameters: viscosity of the fluid (μ), radius of the oscillator (a), distance between traps for a single oscillator (λ), threshold distance for trap switching (ξ), number of discretization points on the oscillator (N_b), trapping stiffness (κ) and membrane stiffness (KK). The default setting of the parameters with the description is shown in Table 4.1. Discretize the immersed body by N_b points equally placed on the boundary. Set the initial position of the active trap and immersed boundary points. Here we assume the trap and the immersed body have the same shape.
2. Based on the position of immersed boundary points and the trap points, we compute the trapping force $\tilde{\mathbf{F}}_i(t)$ and membrane force $\hat{\mathbf{F}}_i(t)$ for each immersed boundary point $\mathbf{X}_i(t)$, $i = 1, \dots, N_b$. Get $\mathbf{F}(\mathbf{X}_i)$ by adding the two force together, that's the total external force exerted on the position $\mathbf{X}_i(t)$.
3. Apply the velocity formulas (equation (3.4) and (3.5) or (3.12) and (3.13) depend on different scenario) with proper ϵ to get the velocity of the immersed boundary points.
4. Update the position of the immersed boundary points by Euler's method.

$$\mathbf{X}_i(t + \Delta t) = \mathbf{X}_i(t) + \Delta t \mathbf{U}_i(t)$$

Here $\mathbf{U}_i(t)$ is the velocity of the i^{th} immersed boundary point at time t computed in step 3.

5. Compute the centroid of the immersed body. Check if it reaches the threshold distance to the active trap. If it does, then turn off the current trap and activate the other.
6. Go back to step 2 to do another loop of simulation.

description	parameter	value
Fluid viscosity	μ	0.5
Membrane stiffness	K	$10^5 ds$
Trap stiffness	κ	$5 ds$
Distance between the traps for a single oscillator	λ	0.3
Threshold distance to change the trap position	ξ	0.05
Radius of the immersed body	a	0.05
Number of points on the immersed boundary	N_b	40
Initial distance between neighboring IB points	ds	$a \sqrt{2(1 - \cos(\frac{2\pi}{N_b}))}$
Stokeslet parameter	ϵ	$0.5 ds$
Time step	Δt	10^{-4}

Table 4.1: The default setting for dimensionless parameters used in Stokes flow cases.

4.2 Single Oscillator Simulation

1. Convergence Study.

First of all, we would like to check if we are using a proper blob size for the regularized Stokeslet. The temporal period obtained from numerical simulation for ϵ varies from $0.5 ds$ to $2 ds$ is shown in Table 4.2. Compared to the temporal period using the Oseen approximation ($T = 1.8435$), the difference is between 0.5% and 3%. In the following simulations, we choose $\epsilon = 0.5 ds$.

ϵ/ds	0.5	0.6	0.7	0.8	0.9	1.0	1.1	1.2
T	1.8533	1.8563	1.8591	1.8618	1.8645	1.874	1.8699	1.8727
ϵ/ds	1.3	1.4	1.5	1.6	1.7	1.8	1.9	2.0
T	1.8755	1.8783	1.8812	1.8871	1.8901	1.8901	1.8931	1.8962

Table 4.2: The temporal period computed with the choosing of different blob size. Using the same set of parameters, the half temporal period computed using Oseen approximation is 1.8435. Here ϵ is the blob size for Stokeslet, and T represents the half temporal period.

We also checked how the numerical solution depended upon Δt . We varied the time step from 10^{-5} , 5×10^{-5} and 10^{-4} , and compared the temporal period with the Oseen tensor approximation. Table 4.3 shows the difference is within 0.55%.

2. Change parameters to check the code.

Δt	Regularized Stokeslet	Oseen
10^{-5}	1.85327	1.8435
5×10^{-5}	1.85325	1.8435
10^{-4}	1.85330	1.8435

Table 4.3: The half temporal period comparison between regularized Stokeslets and Oseen Approximation, with different dt .

To validate our code, we explored the effects of the parameters λ , ξ and k on the temporal period, and compare with the Oseen solution.

(a) Distance between traps (λ).

Our default setting is $\lambda = 6a$, and $\xi = a$. In this part, we change λ from $3a$ to $10a$, and compare the result of temporal period of oscillation with Oseen tensor approximation. The difference is around 0.5%. The comparison result is shown in Fig 4.2.

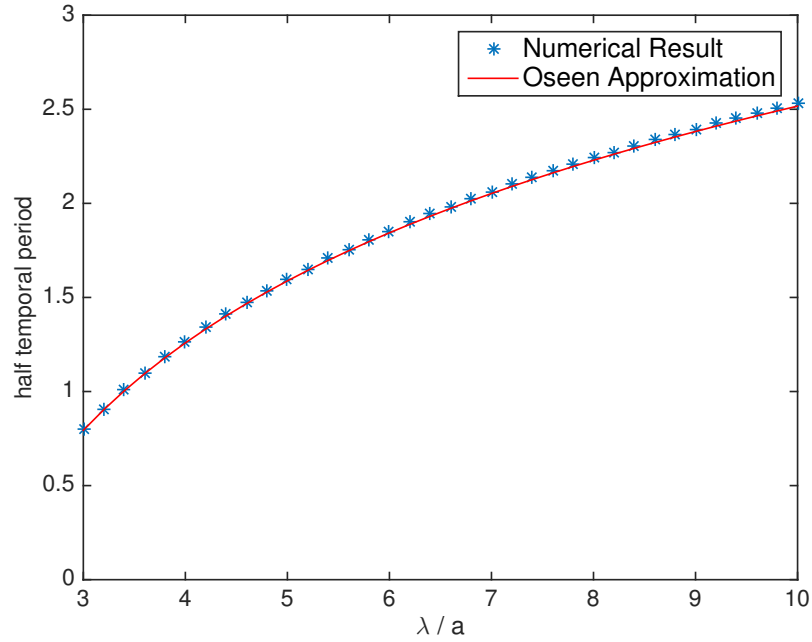


Figure 4.2: The temporal period comparison between regularized Stokeslet and Oseen Approximation, with different distance between traps λ .

(b) Threshold distance (ξ).

The temporal period of oscillation as the threshold distance ξ varies from $0.4a$ to $1.6a$ is shown in Fig 4.3. The comparison result difference is around around 0.62%.

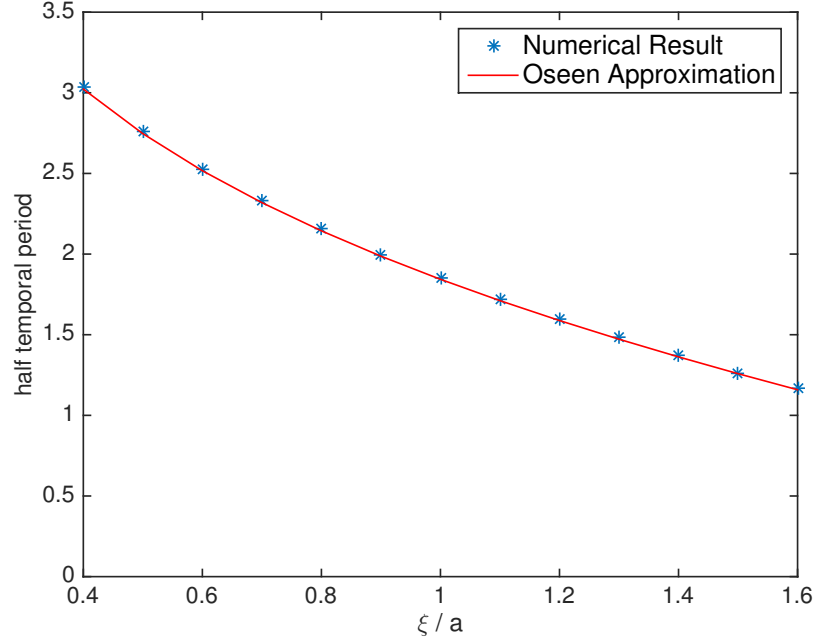


Figure 4.3: The temporal period comparison between regularized Stokeslet and Oseen Approximation, with different ξ .

(c) Trap stiffness (κ).

In this part, we change the trapping stiffness κ from $3 ds$ to $7 ds$, and the temporal period compared with Oseen tensor approximation is shown in Fig 4.4. The comparison result differs around 0.55%.

3. The effect of spatial periodicity.

Here we compare the oscillator in free space to the one with periodic copies to study the effect of periodicity. In this part, we compare the temporal periodicity of oscillator in Stokes free space with two cases:

- (a) Singly periodical oscillators where the oscillating direction is same as the spatial period. In this part, we consider the case that the oscillators lies on

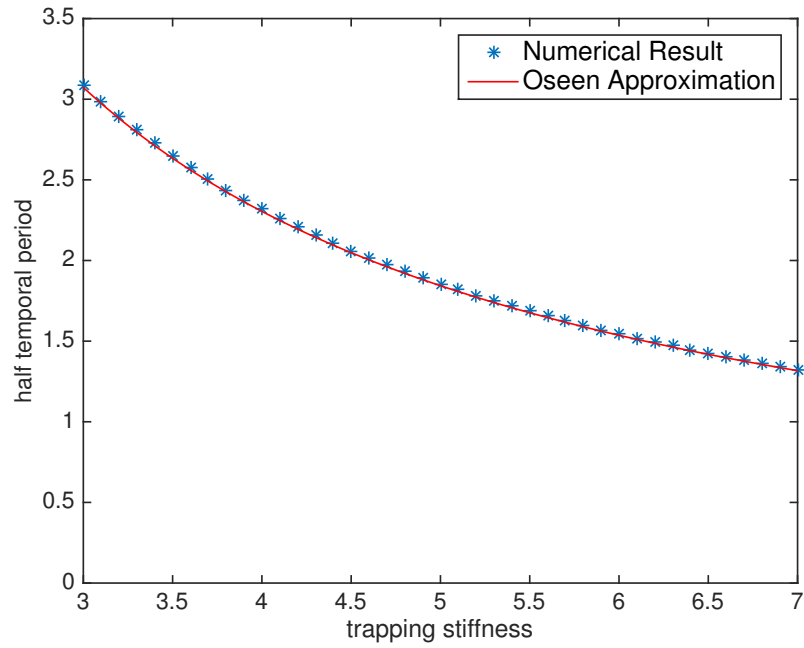


Figure 4.4: The temporal period comparison between regularized Stokeslet and Oseen Approximation, with different trapping stiffness κ .

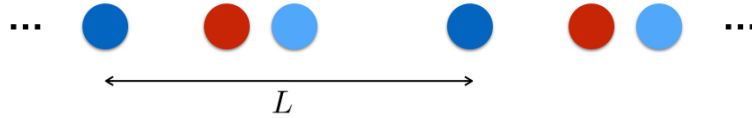


Figure 4.5: The spatial period is same as oscillating direction. Here L is the spatial periodicity.

x -axis, and they also oscillate in x -direction. An illustration graph for this situation is shown in Fig 4.5. We run cases for spatial period L from $20a$ to $80a$, where a is the radius of the oscillator. The comparison between singly periodic and free space regularized Stokeslet temporal periodicity is shown in Fig 4.6, the maximum difference between them is 0.25%.

A periodic line of oscillators exhibit a longer temporal period than the single one in free space. As the oscillators get closer, the temporal period increases.

We conjecture that this is consistent with the anti-phase stability of two oscillators coupled in Stokes fluid in free space. By introducing periodicity in x -direction, the neighboring oscillators are forced to move exactly in-phase. However, the nature of the neighboring oscillators in free space tend to be anti-phase. This conflict of interest makes the temporal period of the singly periodic case larger than in free space.

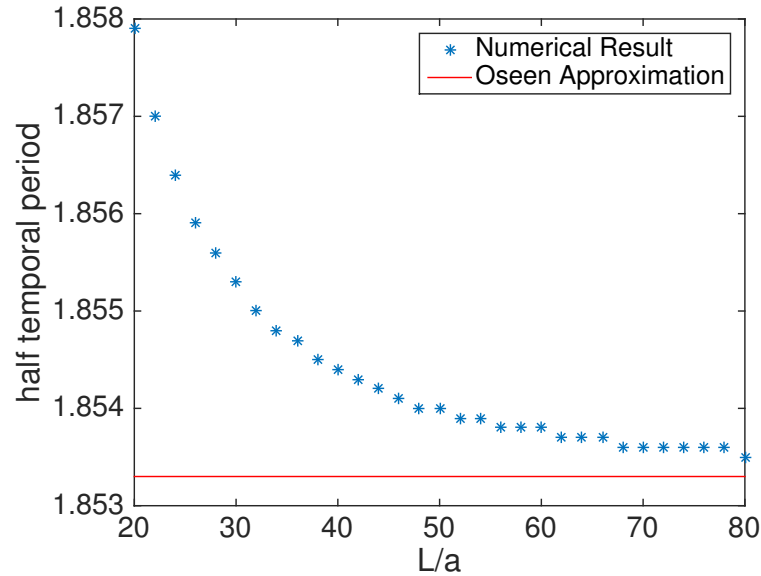


Figure 4.6: The temporal period comparison between singly periodic oscillators case (a) and single oscillator in Stokes free space.

(b) Singly periodical oscillators where the oscillating direction is orthogonal to

the spatial period. In this part, we consider the case that the oscillators

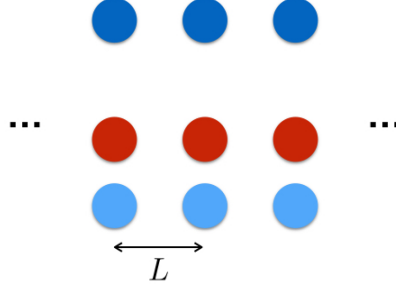


Figure 4.7: The spatial period is orthogonal to the oscillating direction. Here L is the spatial periodicity.

oscillate in y -direction, while they are periodic in x -direction. An illustration graph for this situation is shown in Fig 4.7. To avoid the Stokes paradox, we change the spatial periodicity from $3a$ to $10a$ (a is the radius of the oscillator), not too close so the neighboring oscillators can overlap, nor too large that the Stokes paradox may involved. The comparison of temporal periodicity is shown in Fig 4.8.

As the oscillators get closer, the temporal period decreases. This is consistent with the two oscillators study when the oscillators are vertically placed. The periodicity can be seen as exact in-phase, and the numerical simulation of two vertically placed oscillators shows that the exact in-phase initial setting is stable. When the neighboring oscillators are closer, they oscillate more quickly.

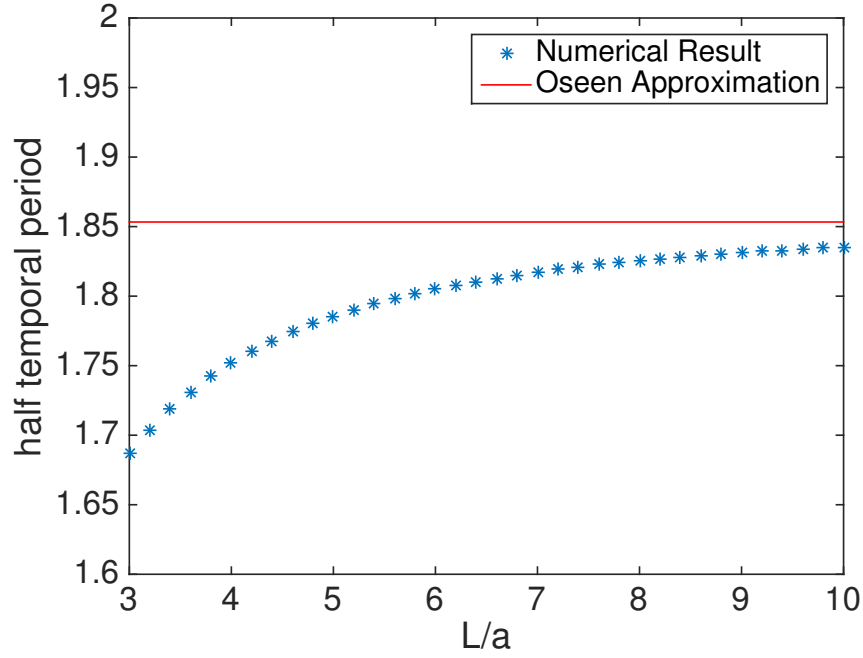


Figure 4.8: The temporal period comparison between singly periodic oscillators case (b) and single oscillator in Stokes free space.

4.3 Two Oscillators

Here, we study the coupling of two oscillators in three scenarios in free space.

1. Parallel placed oscillators.

We assume two oscillators are placed on x -axis and they also moving in x -direction, this is the same assumption as in [4]. We assume the trap positions are listed in table 4.4, and the four cases we study are listed in table 4.5.

Trap ID	Centroid position
$T_{(1,-1)}$	(0,0)
$T_{(1,1)}$	(0.3, 0)
$T_{(2,-1)}$	(0.5, 0)
$T_{(2,1)}$	(0.8, 0)

Table 4.4: The setting of trap position.

The snapshots of the exact in-phase case is shown in Fig 4.9. At $t = 0$, the two oscillators are placed exact in-phase and both are moving left. At $t = 0.6$,

Initial Setting	Oscillator 1	$T_{1,active}$	Oscillator 2	$T_{2,active}$
Exact in-phase	(0.1, 0)	$T_{(1,-1)}$	(0.6, 0)	$T_{(2,-1)}$
Perturbed in-phase	(0.1, 0)	$T_{(1,-1)}$	(0.61, 0)	$T_{(2,-1)}$
Exact anti-phase	(0.1, 0)	$T_{(1,-1)}$	(0.7, 0)	$T_{(2,1)}$
Perturbed anti-phase	(0.1, 0)	$T_{(1,-1)}$	(0.69, 0)	$T_{(2,1)}$

Table 4.5: The initial setting of four cases.

the right one switches direction first while the one on the left still moving left. The left oscillator keep trying to move left, while the right one generates a large velocity field toward right to prevent the left one from reaching the threshold distance to the active trap. Around $t = 2.2$, the left oscillator about to switch direction and lead the the two oscillators show an perturbed anti-phase position. Later, the two oscillators behave like the perturbed anti-phase case and goes to exact anti-phase coupling.

We do simulations for these four cases, and get the shifted centroid plotted in Fig 4.10. To quantify the coupling state of the two oscillators, we study

$$Q_{1,2}(t, 0.5) = \frac{\langle x_1, x_2 \rangle}{||x_1|| ||x_2||}$$

The computed Q for four cases are plotted in Fig 4.11.

2. Vertically placed oscillators.

We also study the case where the moving directions of two oscillators are orthogonal to the direction on which the oscillators are placed. We assume the oscillators are moving in x -direction, and the two oscillating systems are centered on y -axis. The setting of trap positions are listed in table 4.6. We placed the two oscillators close in the vertical position to avoid Stokes paradox. The initial setting of the four cases we study are listed in table 4.7.

The numerical simulation of four cases shows that the exact in-phase case keeps

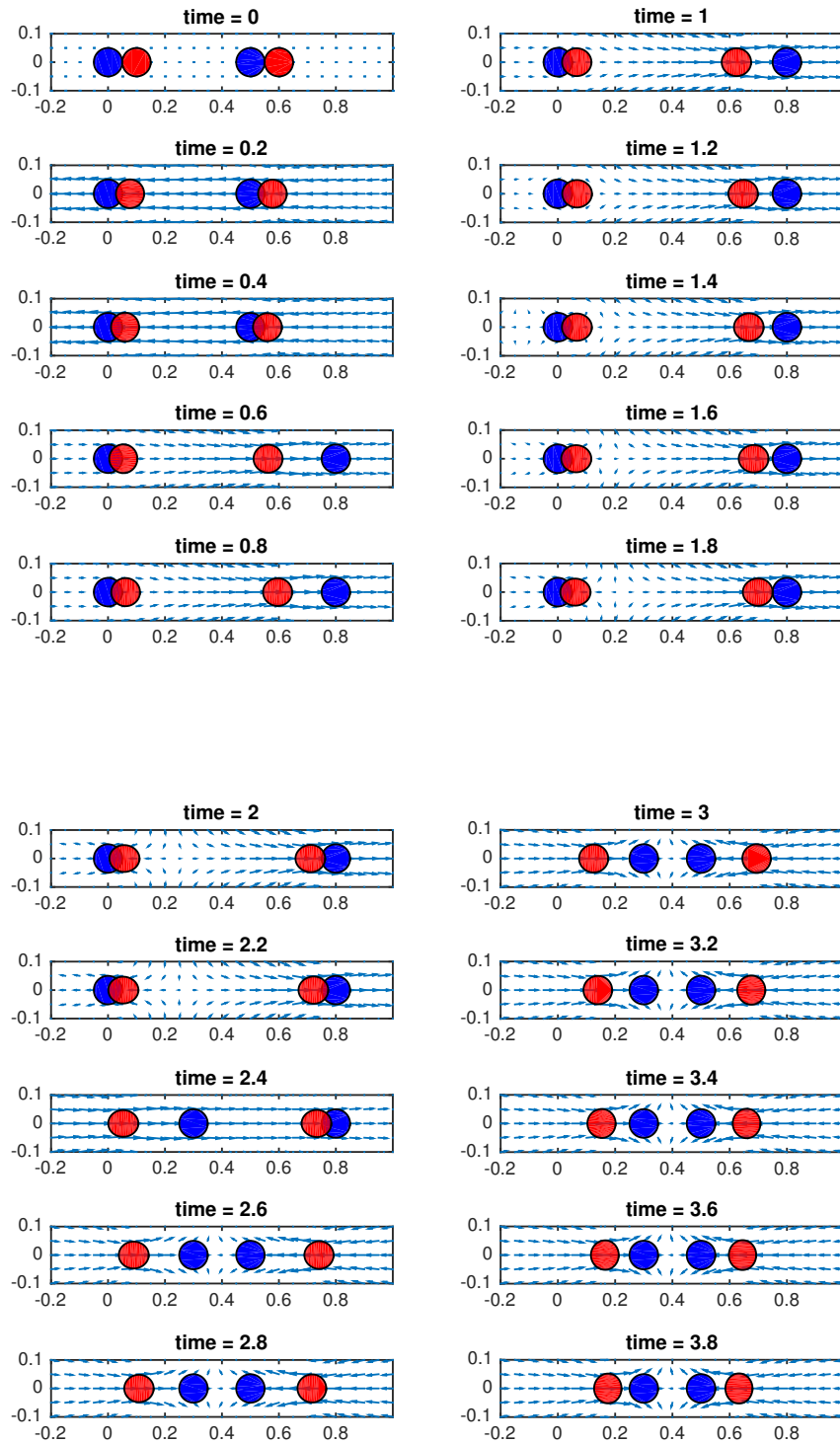


Figure 4.9: Snapshot of two oscillators coupling through fluid. Initially set to be exact in-phase state, and the coupling goes to anti-phase.

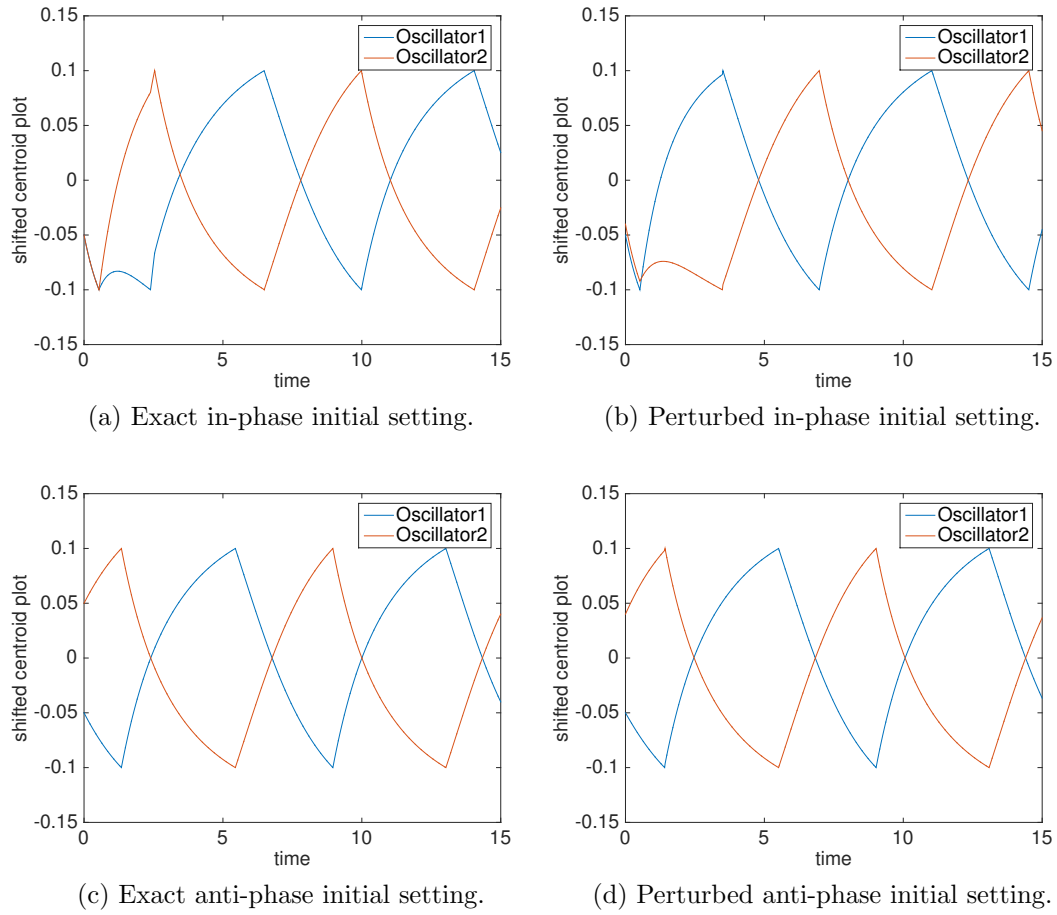


Figure 4.10: The shifted centroid plot of four cases of parallel placed oscillators. All four cases go to anti-phase.

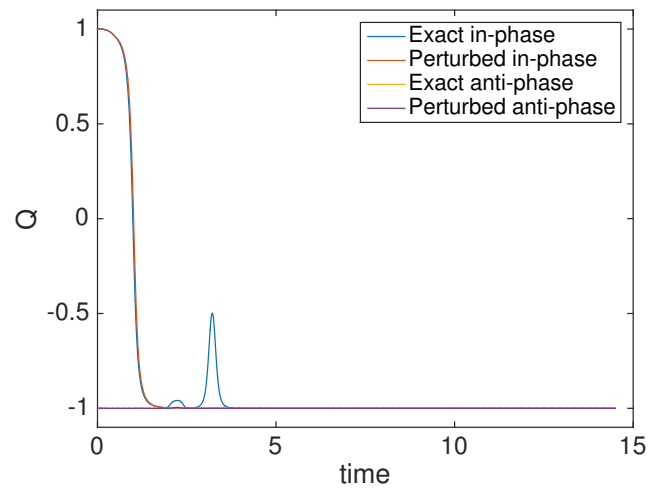


Figure 4.11: Coupling indicator for four cases, parallel placed oscillator.

Trap ID	Centroid position
$T_{(1,-1)}$	(0,0)
$T_{(1,1)}$	(0.3, 0)
$T_{(2,-1)}$	(0, 0.3)
$T_{(2,1)}$	(0.3, 0.3)

Table 4.6: The setting of trap position.

Initial Setting	Oscillator 1	$T_{1,active}$	Oscillator 2	$T_{2,active}$
Exact in-phase	(0.1, 0)	$T_{(1,-1)}$	(0.1, 0.3)	$T_{(2,-1)}$
Perturbed in-phase	(0.1, 0)	$T_{(1,-1)}$	(0.11, 0.3)	$T_{(2,-1)}$
Exact anti-phase	(0.1, 0)	$T_{(1,-1)}$	(0.2, 0.3)	$T_{(2,1)}$
Perturbed anti-phase	(0.1, 0)	$T_{(1,-1)}$	(0.19, 0.3)	$T_{(2,1)}$

Table 4.7: The initial setting of four cases.

in-phase, and all other cases goes to anti-phase. The centroid plots are shown in 4.12 and the coupling indicator is shown in 4.13. Here, round-off error does not alter the exact in-phase equilibrium solution. However, a small perturbation will change it to anti-phase. The snapshots in Fig 4.14 shows the transition of the perturbed in-phase case to anti-phase state. A snapshot of the flow field in a larger domain at $t = 1$ is plotted in Fig 4.15.

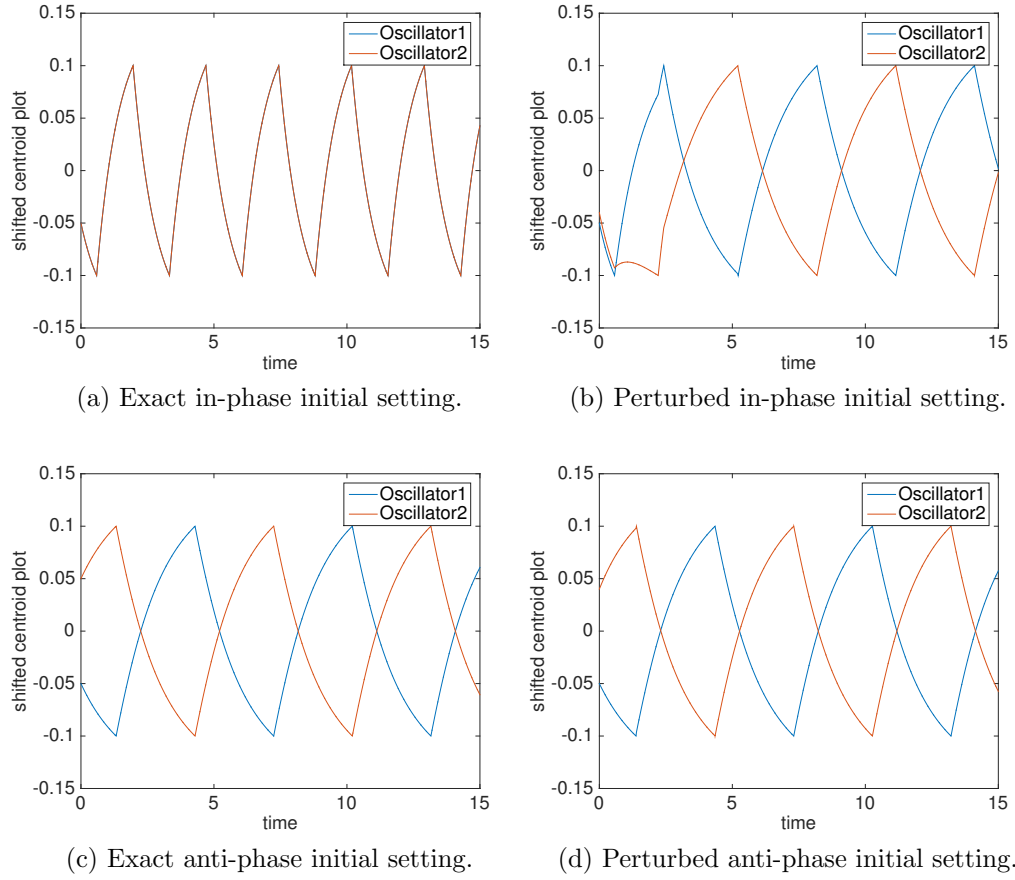
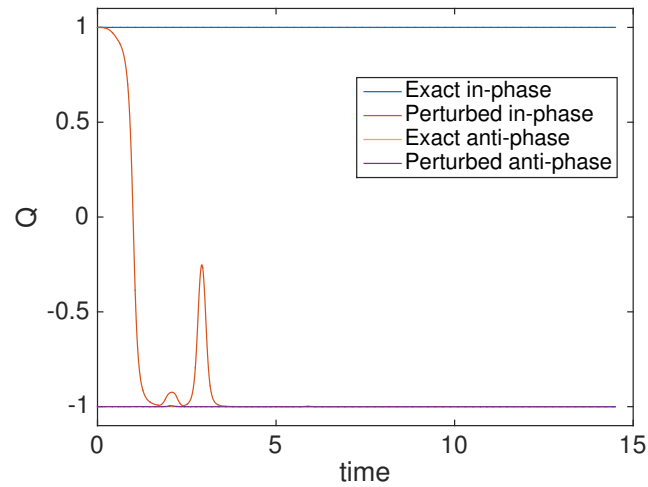


Figure 4.12: The shifted centroid plot of four cases of vertical placed oscillators. The exact in-phase case keeps in-phase, all others go to anti-phase.



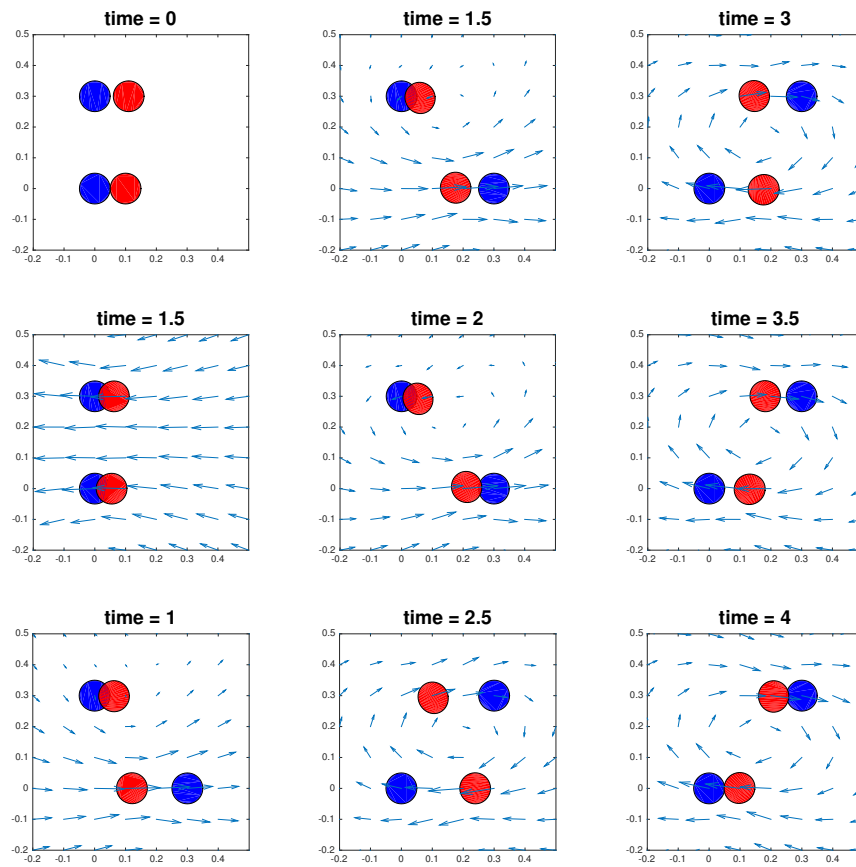


Figure 4.14: Snapshots of perturbed in-phase case.

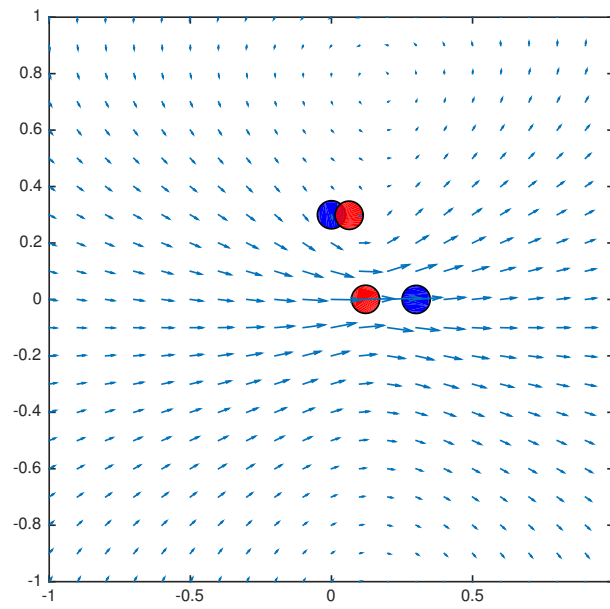


Figure 4.15: Snapshot of perturbed in-phase case at $t = 1$ for a larger domain.

3. Horizontal-vertical oscillators.

Here, we assume oscillator 1 is vertically placed and moving in the y -direction, and oscillator 2 is horizontally placed and moving in the x - direction.

Based on the setting of two oscillators, the in-phase or anti-phase states of two oscillators depend on our choice of the positive direction. However, we can still study if they are coupled or not. If the Q we evaluated is close to 1 or -1, we can say they are synchronized.

The trap positions are set as in table 4.8. Here d is variable to study how the distance between the oscillators affects the locomotion of oscillators. We use the same set of initial position: Oscillator 1 is centered at $(0, 0.11)$ and attracted by $T_{(1,1)}$, Oscillator 2 is centered at $(d + 0.1, 0)$ and attracted by $T_{(2,-1)}$.

Trap ID	Centroid position
$T_{(1,-1)}$	$(0, -0.15)$
$T_{(1,1)}$	$(0, 0.15)$
$T_{(2,-1)}$	$(d, 0)$
$T_{(2,1)}$	$(d + 0.3, 0)$

Table 4.8: The setting of trap position.

We study three cases of $d = 0.3$, $d = 0.5$ and $d = 0.8$. The trajectory of the oscillators are shown in Fig 4.16. Oscillator 1 shows larger deviation from the center line than oscillator 2. And when they are further away, the deviation getting smaller.

When we study the synchronization state, we assume the vertical oscillator rotates clockwise by 90 degree to compare with the horizontal one. Using the projection of two oscillators on their oscillating direction, we compute the synchronization state shown in Fig 4.17. Notice the range of Q varies from -0.975 to -1, this indicates all three cases goes close to anti-phase. When oscillator 1 reaches the bottom position, oscillator 2 is farthest away from oscillator 1. When

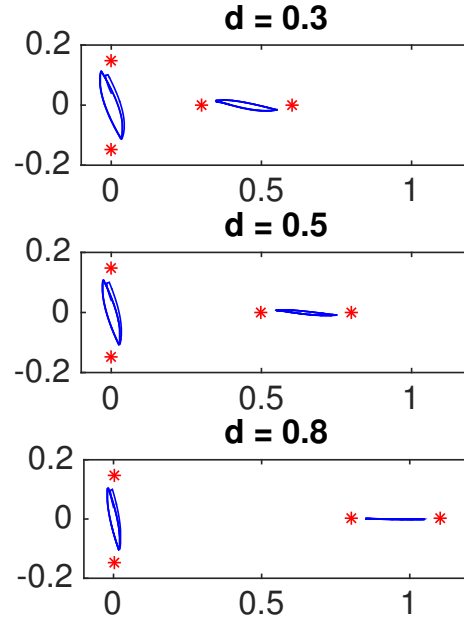


Figure 4.16: Trajectory of oscillators with different d . Here the trajectory is shown in blue, and the possible trap positions are shown in red.

oscillator 1 reaches the top position, oscillator 1 is closest to oscillator 1. The snapshot of $d = 0.3$ case is shown in Fig 4.18. A snapshot of the velocity field in a larger domain at $t = 1$ is shown in Fig 4.19.

4.4 Multiple Oscillator

In this part, we study the cases where three immersed bodies are placed along the same line and the oscillating direction is same as the line. The distance between the neighboring oscillators are set to be the same. An illustration figure showing the position of the oscillators is shown in Fig 4.20.

1. The three immersed bodies all have driven force.

The shifted centroid plot of three oscillators is shown in Fig 4.21, the indicators $Q_{(1,2)}$, $Q_{(1,3)}$ and $Q_{(2,3)}$ are shown in Fig 4.22. We observe the neighboring oscillators tend to go anti-phase, while the two lateral oscillators tend to go

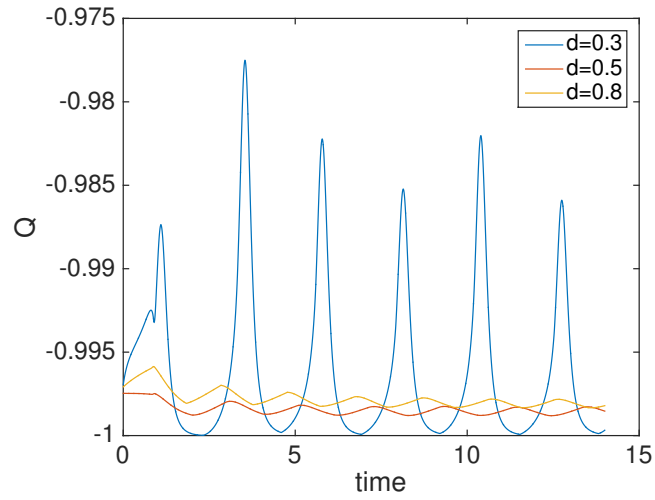


Figure 4.17: Coupling indicator for different d . All three cases go close to anti-phase.

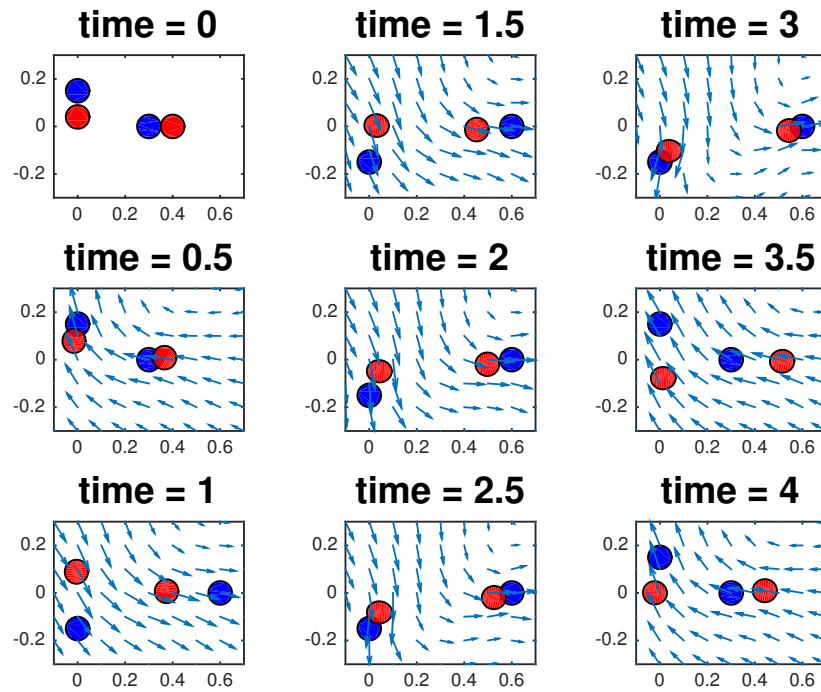


Figure 4.18: Snapshots of two oscillators placed in horizontal-vertical group.

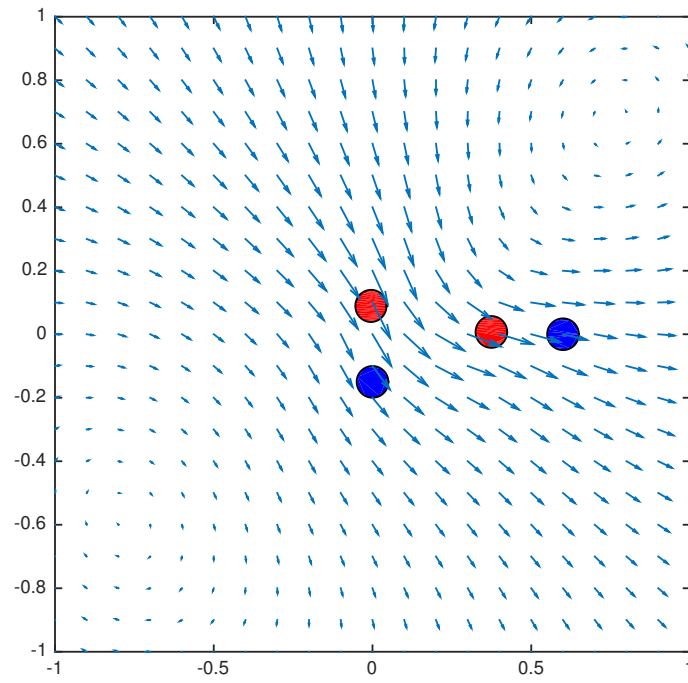


Figure 4.19: Snapshot of two oscillators placed in horizontal-vertical group at $t = 1$.



Figure 4.20: Illustration figure of three oscillators with random initial condition.

in-phase.

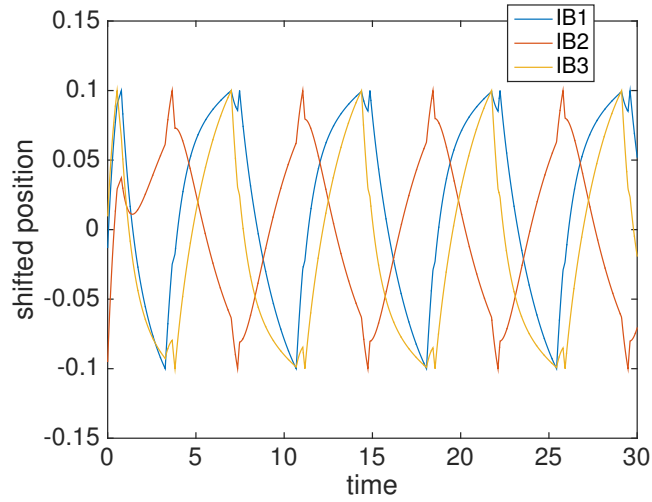


Figure 4.21: Shifted centroid plot for three oscillators.

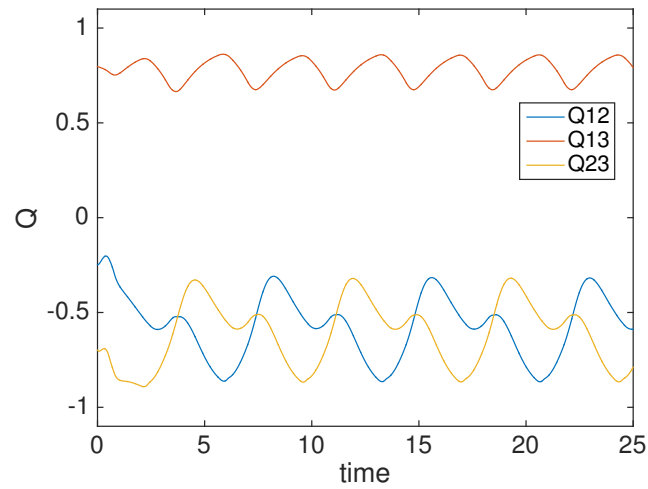


Figure 4.22: Coupling indicator Q . $Q_{(1,3)}$ greater than zero shows the two lateral oscillators tend to go in-phase, while $Q_{(1,2)}$ and $Q_{(2,3)}$ less than zero shows the middle oscillator tends to go anti-phase to the lateral ones.

2. Only the two lateral ones are driven, the one in the middle is passively moving with the fluid.

In this case, the oscillator in the middle could be seen as an indicator in the fluid. The shifted centroid plot is shown in Fig 4.23, and the corresponding indicator plot is shown in Fig 4.24. The previous case of three driven oscillators

can be seen as adding a third oscillator to the two oscillator coupled system, and the third oscillator dramatically changes the coupling state of the original two. Without the oscillator in the middle, the two oscillators IB1 and IB3 have an anti-phase coupling. By adding the oscillator in the middle, both IB1 and IB3 are anti-phase to IB2, which is the oscillator in the middle. And their coupling state change from anti-phase to in-phase.

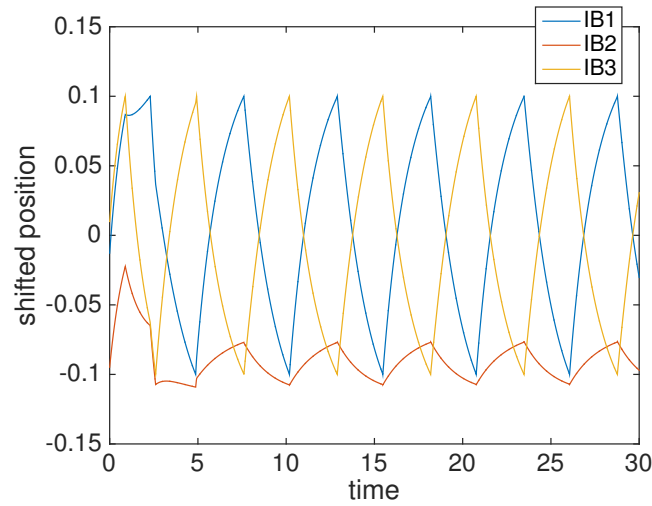


Figure 4.23: Shifted centroid plot for three oscillators.

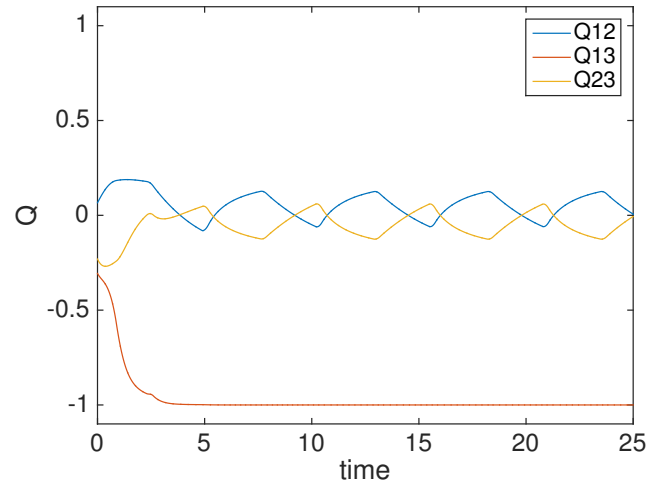


Figure 4.24: Coupling indicator Q . $Q_{(1,3)} = -1$ shows the two lateral oscillators are exact anti-phase, while $Q_{(1,2)}$ and $Q_{(2,3)}$ around zero indicates the middle oscillator just passively move with the fluid.

Chapter 5

Navier Stokes Flow

In this chapter, we discuss the oscillators' behavior in the presence of inertia. The mathematical model is discussed in Chapter 2.

The fluid motion is described by Navier-Stokes equation (2.1) with incompressibility condition (2.2). The body-fluid interaction between the immersed body and the surrounding fluid is described by (2.3) and (2.4). And the force exerted on the immersed body is described by (2.5) to (2.8).

5.1 Numerical Background

In this section, we introduce the numerical methods to solve our problem.

5.1.1 The Immersed Boundary Method

The immersed boundary method was first introduced by Charles Peskin in [25] to simulate the flow patterns around heart valves. The essential idea of this method is to treat the fluid and the immersed body with two different frames. The immersed body is described in a Lagrangian frame (which moves with the fluid), and the surrounding fluid is described in an Eulerian frame (which spatially fixed) [26].

We describe the fluid domain D using a regular, finite difference mesh with $\Delta x = \Delta y$. Periodic boundary condition is imposed. We describe the immersed body by N_b points on its boundary. The points on the immersed boundary are described as \mathbf{X}_s^k , where s is a Lagrangian index that goes from 1 to N_b , and k means the k^{th} time step. The spreading of the force is based on (2.3). In each time step, we spread the force exerted by each immersed boundary point to the nearby fluid mesh points within 2 cell size by blob function (5.1),

$$\Phi_h(r) = \frac{1}{4\Delta x} \left(1 + \cos\left(\frac{\pi r}{2\Delta x}\right) \right) \quad (5.1)$$

For example, the force \mathbf{F}_s^k is exerting on the immersed boundary point $\mathbf{X}_s^k = (X_s^k, Y_s^k)$, and \mathbf{X}_s^k is located in the cell of fluid mesh formed by $\mathbf{x}_{(i,j)}$, $\mathbf{x}_{(i,j+1)}$, $\mathbf{x}_{(i+1,j)}$ and $\mathbf{x}_{(i+1,j+1)}$. The the force $\mathbf{F}_{(s,k)}$ is spread to the mesh points $\mathbf{x}_{m,n} = (x_m, y_n)$ ($i-1 \leq m \leq i+2$, $j-1 \leq n \leq j+2$) with the weight $w_{m,n}$ given by (5.2).

$$w_{m,n} = \left(\frac{1}{4\Delta x} \left(1 + \cos\left(\frac{\pi(X_s^k - x_m)}{2\Delta x}\right) \right) \right) \cdot \left(\frac{1}{4\Delta x} \left(1 + \cos\left(\frac{\pi(Y_s^k - y_n)}{2\Delta x}\right) \right) \right). \quad (5.2)$$

The spread force at the point $\mathbf{x}_{m,n}$ is

$$\mathbf{f}_{m,n}^k = w_{m,n} \mathbf{F}_s^k. \quad (5.3)$$

After the computation of force spreading in each time step, we compute the velocity at each fluid mesh point, and then we interpolate back the velocity from the grid to get the velocity of the immersed body by (2.4) using the same blob function. We get the velocity \mathbf{U}_s^k of \mathbf{X}_s^k at time step k by (5.4).

$$\mathbf{U}_s^k = \sum_{i-1 \leq m \leq i+2, j-1 \leq n \leq j+2} w_{m,n} \mathbf{u}_{m,n}^k \quad (5.4)$$

5.2 Computation Steps

In this section, we describe what we do in each time step. At the very beginning, we initialize the parameters as in the Stokes case. Also, we descretize the fluid to mesh points and set the initial velocity field of the fluid to be zero everywhere. We assume at the beginning of time step k , we have the position of the active trap points $\mathbf{T}_s^k = (Tx_s^k, Ty_s^k)$, position of the immersed boundary points $\mathbf{X}_s^k = (x_s^k, y_s^k)$ where s goes from 1 to N_b . We also have the velocity $\mathbf{u}_{i,j}^k = (u_{i,j}^k, v_{i,j}^k)$ on the mesh points $\mathbf{x}_{i,j} = (x_{i,j}, y_{i,j})$ in the fluid where $1 \leq i, j \leq N$, and N is the number of points on each side of the evaluated domain.

Here are the things we do in the following order in time step k ,

1. Find the force exerted on immersed boundary points.

Compute the external force acting on the immersed boundary points, based on the positions of the immersed boundary points and the acting trap points. The total force acting on immersed body is composed of two part: membrane force \mathbf{Fm} and trap force \mathbf{Ft} .

$$\mathbf{F}_s = \mathbf{Fm}_s + \mathbf{Ft}_s, \quad s = 1, \dots, N_b$$

Here

$$\begin{aligned} \mathbf{Fm}_s &= K_1((\|\mathbf{X}_{s+1} - \mathbf{X}_s\| - ds)\mathbf{v}_{s+1,s} + (\|\mathbf{X}_{s-1} - \mathbf{X}_s\| - ds)\mathbf{v}_{s-1,s}) + \\ &\quad K_2 \cdot ((\|\mathbf{X}_{s+2} - \mathbf{X}_s\| - ds_2)\mathbf{v}_{s+2,s} + (\|\mathbf{X}_{s-2} - \mathbf{X}_s\| - ds_2)\mathbf{v}_{s-2,s}) \\ \mathbf{Fm}_s &= \kappa \cdot (\mathbf{T}_s - \mathbf{X}_s) \end{aligned}$$

Here $\mathbf{v}_{i,j}$ is the normalized vector defined by

$$\mathbf{v}_{i,j} = \frac{\mathbf{x}_i - \mathbf{x}_j}{\|\mathbf{x}_i - \mathbf{x}_j\|}$$

Since both the immersed body and the trap are closed, we use $\mathbf{X}_{N_b+j} = \mathbf{X}_j$, $\mathbf{T}_{N_b+j} = \mathbf{T}_j$, $j = 1, 2$. Here K_1 is the tensile spring stiffness, K_2 is the bending spring stiffness, κ is the trapping stiffness. ds is the rest length for the neighboring immersed boundary points, and ds_2 is the rest length for the next neighboring immersed boundary points. For simplicity, we assume $K_1 = K_2 = K$.

2. Spread the exerted force to fluid mesh points.

Spread the force acting on the immersed boundary points to the surrounding fluid mesh points based on equation (2.3) using (5.3). In this step, we can get $\mathbf{f}_{i,j}$ for $1 \leq i, j \leq N$.

3. Solve the discretized Navier-Stokes equation on the regular, periodic grid using Fast Fourier transforms [27].

An upwind scheme was used for the convection term, and centered differences for other terms.

4. Compute velocities of immersed boundary points.

Get the velocity of the immersed boundary points by equation (2.4). Numerically we do interpolation given by (5.4) to get \mathbf{U}_s^{k+1} ($1 \leq s \leq N_b$) from $\mathbf{u}_{i,j}^{k+1}$ ($1 \leq i, j \leq N$).

5. Update the position of the immersed body.

Here we use forward-Euler method to update the immersed body by

$$\mathbf{X}^{k+1}(s) = \mathbf{X}^k(s) + \Delta t \mathbf{U}^{k+1}.$$

6. Check if we need to switch the acting trap.

If we have

$$|\bar{\mathbf{T}}^k - \mathbf{X}^{\bar{k}+1}| < \xi,$$

here $\bar{\mathbf{T}}^k$ and $\mathbf{X}^{\bar{k}+1}$ represent the centroid of the trap and immersed body respectively, we turn off the acting trap and turn on the other one.

The operations in this time step is finished and start over for the next time step.

In the case of Stokes flow in a domain D with doubly periodic boundary conditions, there is a compatibility condition of the force applied on the domain. These forces must integrate to zero over D . This is easily seen by integrating the equation over the periodic cell. For instance, such a constraint is met by the force generated by free microswimmers [28]. However, the trap forces used in our model oscillator are external forces that do not sum to zero. This compatibility condition did not arise in the previous chapter, since doubly-periodic boundary condition were not used. For Stokes immersed boundary models, where periodic boundary condition were used for simplicity, modifications to the algorithm have been introduced in [27, 29].

It have been noted that problems with this condition may appear when solving the Navier-Stokes equation numerically on a doubly-periodic domain in the presence of external forces that do not integrete to zero at very low Reynolds number [29].

5.3 Numerical Simulation for a Single Oscillator.

First, we study the case of single oscillator in 2×2 doubly periodic Navier-Stokes fluid and compare it with the case of an oscillator in free Stokes fluid. The default setting of the parameters are listed as in table 5.1.

5.3.1 Convergence study

1. Check for dt .

The first thing we would like to make sure is whether we are using a reasonable dt . We run cases with the same initial setting with $dt = 10^{-4}$ and $dt = 10^{-5}$,

description	parameter	value
Spatial periodicity	L	2
Distance between the traps for a single oscillator	λ	0.3
Threshold distance to change the trap position	ξ	0.05
Spatial mesh size	Δx	$\frac{1}{2^6}$
Number of mesh point on each side for a spatial period	N	L/dx
Radius of the immersed body	a	0.05
Time step	dt	10^{-4}
Fluid viscosity	μ	1
Fluid density	ρ	10
Number of points on the immersed boundary	N_b	40
Spring stiffness between the IB points	K	10^5
Spring stiffness between the IB point and the trap	κ	5

Table 5.1: The default setting for dimensionless parameters used in Navier-Stokes cases.

the difference between these two cases is within 0.01%. Our default time step is therefore chosen to be $dt = 10^{-4}$.

2. Check for dx .

Another thing we check is if we discretize the space properly. For the same immersed body, we discretize the boundary to equally spaced points. We check the discretization of 40, 80 and 160 points for the immersed boundary, and change the mesh grid size of fluid corresponding to them. For the domain $D = [0, 2] \times [0, 2]$, we choose a 128×128 , 256×256 and 512×512 grid, so ds/h is about 0.5. The centroid plot is shown in Fig 5.1 with the moving trajectory of the centroid of the immersed body starting at the same initial position for a 0.5s time period. The maximum difference between the displacement of the trajectory of three cases is within 0.3%.

To study the spatial convergence rate, we denoted the centroid position of oscillator as $x_{40}(t)$, $x_{80}(t)$ and $x_{160}(t)$ corresponding to $N_b = 40, 80, 160$. We also assume $x_{160}(t)$ is close enough to the exact solution. Without changing other

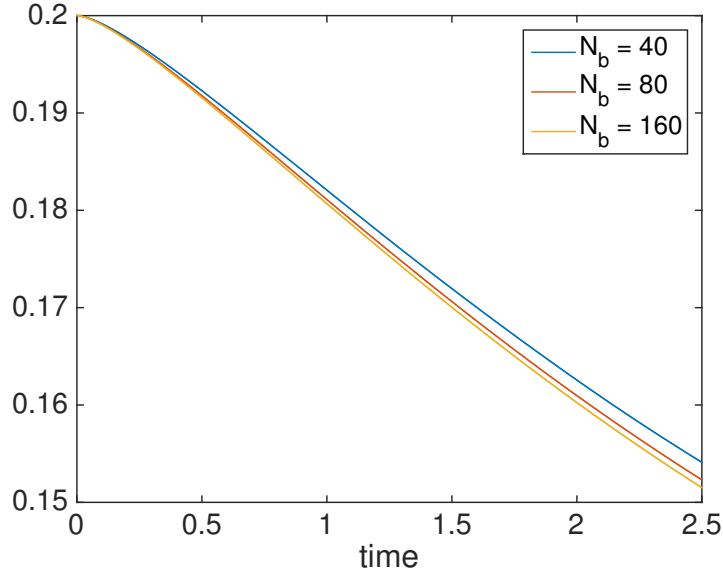


Figure 5.1: Centroid plot of single oscillator with different N_b .

parameters, we have

$$\begin{aligned} \|x_{40} - x_{160}\| &:= |x_{40}(T) - x_{160}(T)| Ch^p \\ \|x_{80} - x_{160}\| &:= |x_{80}(T) - x_{160}(T)| C\left(\frac{h}{2}\right)^p \end{aligned}$$

Here $T = 2.5$ is the final time of our computation period, C is a constant, h is the distance between neighboring immersed boundary points, and p is the convergence rate. p can be computed by

$$p = \frac{1}{\log 2} \log \left(\frac{\|x_{40} - x_{160}\|}{\|x_{80} - x_{160}\|} \right).$$

$p = 1.75$ in our study.

5.3.2 Inertia affects the oscillator motion

In order study how inertia affect the locomotion of the oscillator, we change ρ to change Reynolds number, and the Reynolds number is computed by (5.5). Here u_{max} is the maximum velocity through the whole simulation process, thus Reynolds number (Re) is computed at the very end of each simulation.

$$Re = \frac{\rho a u_{max}}{\mu} \quad (5.5)$$

5.3.3 Modify Re by changing fluid density ρ

We assume doubly periodic boundary condition for the Navier-Stokes case to use discrete fast Fourier transform. By varying ρ to change Re , we have the simulated temporal period for oscillator in Navier-Stokes fluid and the compared temporal period with same parameters for Oseen solution in free space in Stokes fluid as shown in Fig 5.2. We would like to see the temporal period in the Navier-Stokes case approach the Stokes case as $Re \rightarrow 0$.

Note that without inertia, an oscillator should never overshoot its target position. When such overshoot occurs at low but nonzero Reynolds number, it is an indication that the numerical solution is polluted because of the non-zero sum of forces in the doubly-periodic domain. Fig 5.2 shows the temporal period for the oscillator in unbounded Stokes fluid with dash line, and the blue curve represents the temporal period for the oscillator corresponding to the same set of parameters in the Navier-Stokes case. The red curve represents the overshoot of the oscillator related to different Re , and is scaled by the radius of the oscillator a . In the overshooting part, the oscillator moves in the opposite direction to the trapping force direction, this is due to the presence of inertia, and the overshoot should increase with Re . However, the overshoot plot is non-physical for very small Re in our simulation. When $Re = 0$, the fluid becomes Stokes fluid, and there should be no overshoot for the oscillator. However,

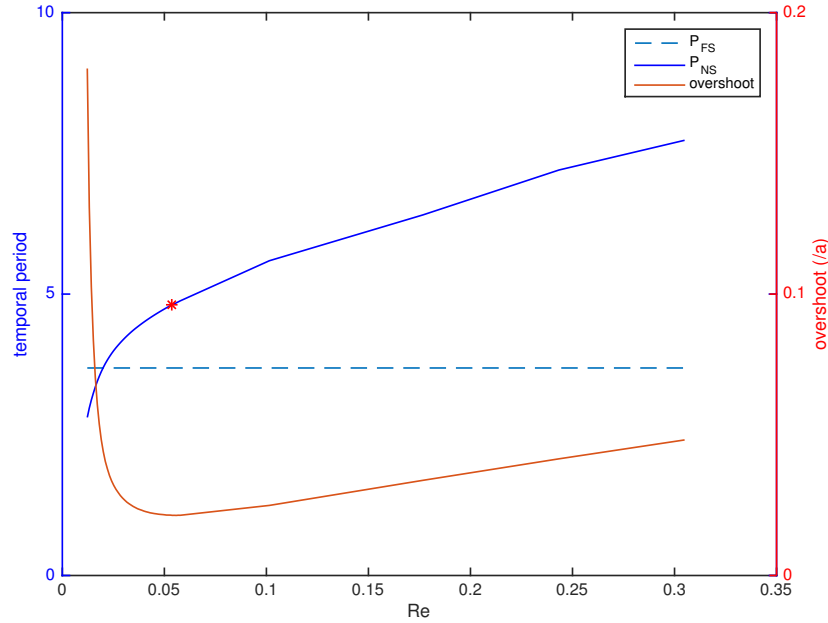


Figure 5.2: Single oscillator in Navier-Stokes fluid.

in our simulation, the overshoot increases as Re gets closer to zero for very small Re . We note that the conflict comes from the doubly-period assumption of space and the exerting force. The red point indicates the Re at which minimal overshoot occurs, and the corresponding $\rho = 9.8$. We will modify our algorithm at Re lower than this value as discussed below.

For the Stokes equations on a doubly-periodic domain, the total force should be zero. However, in our simulation,

$$\int_D \mathbf{f} d\mathbf{x} \approx \sum_{s=1}^{N_b} F_s ds \neq 0$$

One way to deal with this conflict is to introduce a uniform force adjustment everywhere on the fluid gird to balance with the total force exerted on the immersed body, so that the total force sums to zero on the periodic domain, as in [29]. With such adjustment, we rerun the simulations and get Fig 5.3. We show results for the case of a domain $D = [0, L] \times [0, L]$ for both $L = 2$ and $L = 4$. Note that temporal

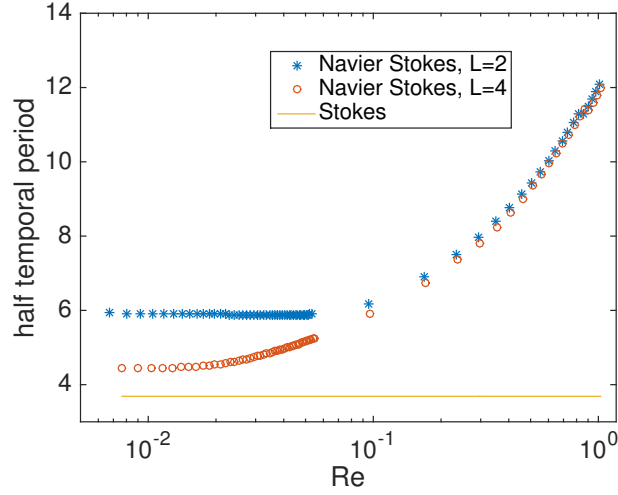


Figure 5.3: Single oscillator in Navier-Stokes fluid, with the adjusted force. Temporal period comparison between cases of Navier-Stokes and free space Stokes.

period of the oscillator on the larger domain $L = 4$ where the modified force per grid point is less than that for $L = 2$ approaches the Stokes period as $Re \rightarrow 0$.

5.3.4 High Re case

When the Re is large, the deformation of the elastic body is observed. Fig 5.4 shows a sequence of snapshots for single oscillator with $Re = 40$. We can observe large deformation in the snapshots of $time = 3$, $time = 8$ and $time = 11$.

5.4 Numerical Simulation for Two Oscillators

Here, we study the coupling of two oscillators in a Navier-Stokes fluid.

The cases we study are two oscillators placed next to each other, and we study the coupling of these two when they are initially set to be exactly in-phase, exactly anti-phase, as well as perturbed in-phase and perturbed anti-phase with different Reynolds numbers.

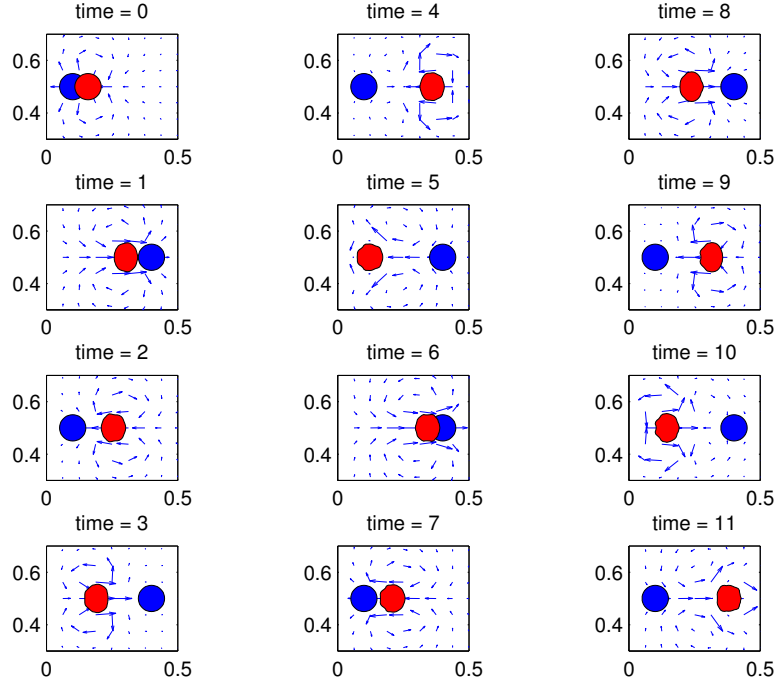


Figure 5.4: For $Re = 40$, the deformation of the elastic body is observed.

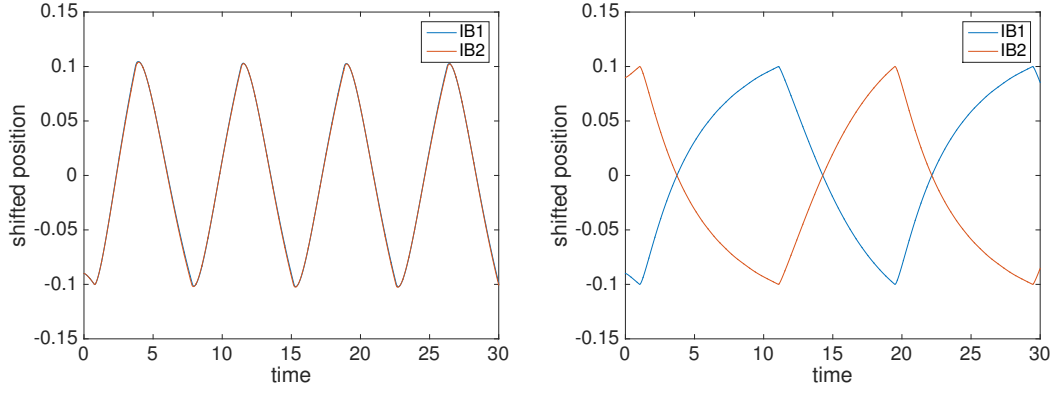
5.4.1 Exactly in-phase / anti-phase case

In the simulations for the exact in-phase and anti-phase initial setting, the two oscillators keep the in-phase / anti-phase state for all Re . A centroid plot for $\rho = 10$ (exactly in-phase state has $Re = 0.08$, and exactly anti-phase has $Re = 0.05$.) case is shown in Fig 5.5.

With this small amount of inertia, the unstable in-phase equilibrium state can remain in-phase, and not goes to anti-phase as in the case of Stokes. This indicates the smoothing of velocity transition at switch times stabilizes the system.

5.4.2 Perturbed in-phase / anti-phase case

In the study of perturbed in-phase and anti-phase study, we set the trap position as in Table 5.2, and the initial setting of exactly in-phase / anti-phase is defined in Table 5.3.



(a) Exact in-phase initial setting. $Re = 0.08$ (b) Exact anti-phase initial setting. $Re = 0.05$

Figure 5.5: Both in-phase state and anti-phase state keep in-phase / anti-phase. ($\rho = 10$)

Trap ID	Centroid of trap
$T_{(1,-1)}$	(0.1, 0.5)
$T_{(1,1)}$	(0.4, 0.5)
$T_{(2,-1)}$	(0.6, 0.5)
$T_{(2,1)}$	(0.9, 0.5)

Table 5.2: The setting of trap position.

	$T_{1,active}$	$T_{2,active}$	IB_1	IB_2
Exactly in-phase	$T_{(1,-1)}$	$T_{(2,-1)}$	(0.16, 0.5)	(0.66, 0.5)
Exactly anti-phase	$T_{(1,-1)}$	$T_{(2,1)}$	(0.16, 0.5)	(0.84, 0.5)

Table 5.3: The initial setting of active traps and oscillators positions. IB_i indicates the centroid of immersed body i , $i = 1, 2$.

For the coupling of two oscillators in Stokes fluid in free space, we have shown analytically and numerically that only the anti-phase state is stable and the in-phase state is unstable. However, this is not always the case for Navier-Stokes.

For the same amount of perturbation, by choosing different fluid density ρ to change Reynolds number, the coupling state changes. Without force adjustment, we consider $\rho = 10$ is the smallest reasonable Reynolds number we could use, and examine densities in the range $\rho = 10$ to $\rho = 100$.

To quantify the coupling state, Q is defined as

$$Q = \begin{cases} Q(t, 1), & \text{for } 0 \leq t < 5 \\ Q(t, t - 4), & \text{for } 5 \leq t < 14 \\ Q(t, 10), & \text{for } t \geq 14 \end{cases}$$

We choose a small viewing window ($t = 1$) to capture the initial perturbation part of the coupling, and smoothly transfer to a large viewing window to get the coupling state for a longer period of time. The compared temporal period for free space Stokes case is $T = 7.4$, and our viewing window of $t = 10$ is used to capture the coupling of one temporal period.

1. Perturbed in-phase state.

We perturb the exact in-phase state by 0.01 (which is 5% of the distance for an oscillator can travel) by moving the initial IB_2 to $(0.67, 0.5)$, that is $x_2 - x_1 = 0.01$. We see that at low Reynolds number, the perturbed in-phase case approaches the anti-phase case. However, with the same amount of perturbation, the perturbed in-phase case approaches the in-phase equilibrium for high Reynolds number.

For these two simulations, the centroid plots of two oscillators are shown in Fig 5.6. We observe the overshoot of oscillators in the $Re = 0.43$ case, but the

overshoot is not obvious in $Re = 0.06$ case. We quantify the coupling state by Q in Fig 5.7 (a), which is consistent with our observation. The perturbed in-phase state is unstable at low Reynolds number, and stable at high Reynolds number. A Q plot for $10 \leq \rho \leq 100$ ($0.06 \leq Re \leq 0.43$) with the difference of ρ be 5 is shown in Fig 5.7 (b).

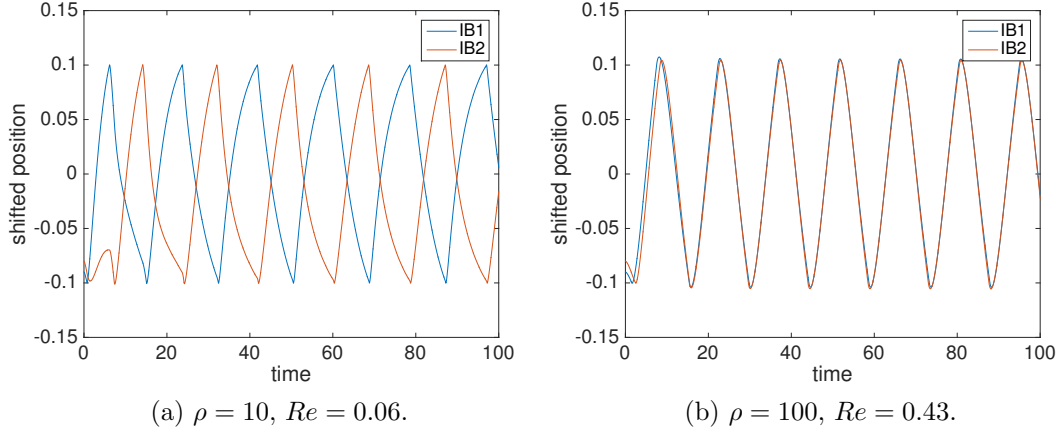


Figure 5.6: Centroid plot for perturbed in-phase state.

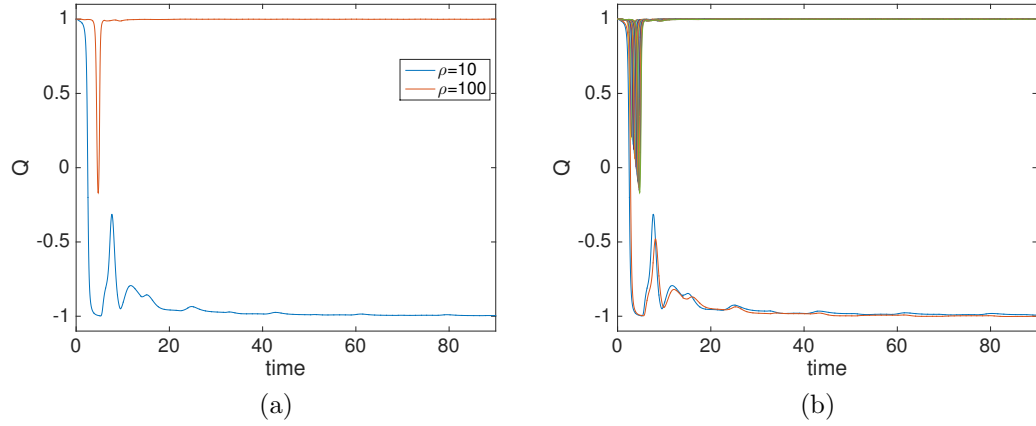


Figure 5.7: Q plot. (a) shows Q plot for $\rho = 10$ ($Re = 0.06$) and $\rho = 100$ ($Re = 0.43$). (b) shows Q plot for $10 \leq \rho \leq 100$ ($0.06 \leq Re \leq 0.43$), with difference of 5 in ρ between each simulation.

We further run a sequence of perturbations by making

$$x_2 - x_1 = 0, 0.01, 0.02, 0.03, 0.04, 0.05,$$

which is from zero perturbation to $0.25(\lambda - 2\xi)$ perturbation. A phase diagram is shown in Fig 5.8. The blue stars indicate that in-phase state was stable with the perturbation shown in y -axis, and Reynolds number in x -axis. The red circles indicate in-phase state was unstable for the given perturbation and Reynolds number. For the time period we run for simulation, the unstable in-phase cases show a tendency to move to anti-phase, but not all of them reach exact anti-phase state due to the limitation of computing time.

The stability region of the in-phase state gets larger as Reynolds number gets larger.

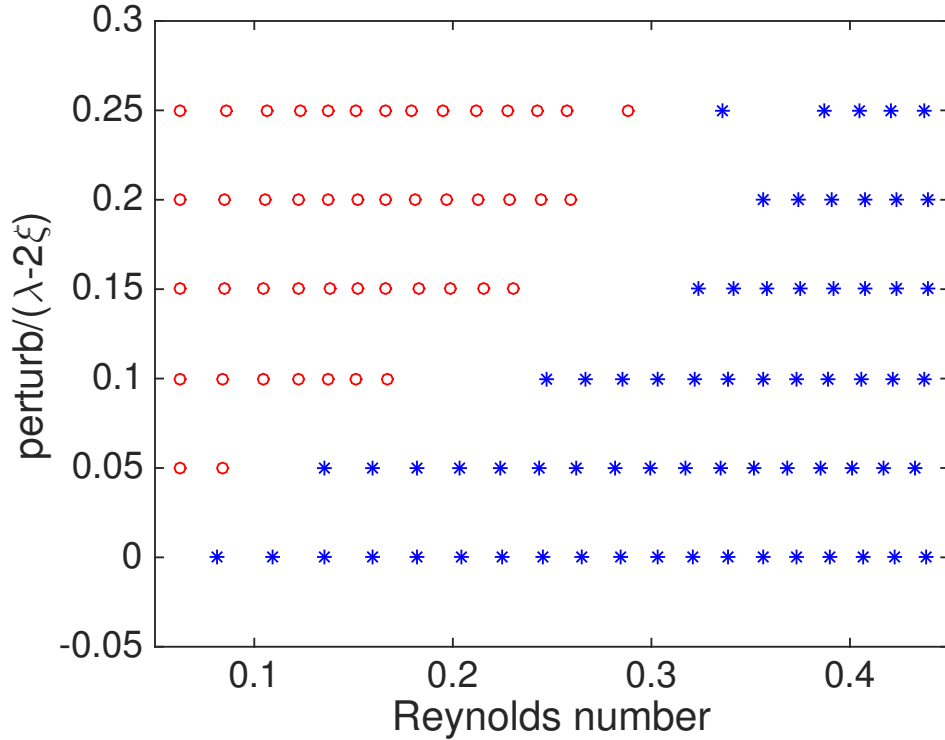


Figure 5.8: Blue stars indicate that in-phase state was stable and red circles indicate that in-phase state was unstable.

2. Perturbed anti-phase state.

Similar to the in-phase case, we do the same stability study for the perturbed anti-phase case. We make IB_2 farther away from the active trap by 0.01, that

is $x_1 + x_2 = -0.01$. The centroid plots are shown in Fig 5.9. We observe more overshoot in $Re = 0.40$ case than $Re = 0.06$ case. The anti-phase state is stable in low Reynolds number cases, and unstable in high Reynolds number cases. The corresponding Q plot is shown in Fig 5.10 (a), and the stability indicator Q is plotted for $10 \leq \rho \leq 100$ ($0.06 \leq Re \leq 0.40$) with the difference of ρ be 5 is shown in Fig 5.10 (b). The red circles indicate that the anti-phase was stable to those perturbations, while the blue stars indicate that the anti-phase was unstable. For the time period we run for simulations, the unstable anti-phase cases showed a tendency to in-phase, but not all of them reach the in-phase state due to the limitation of computing time.

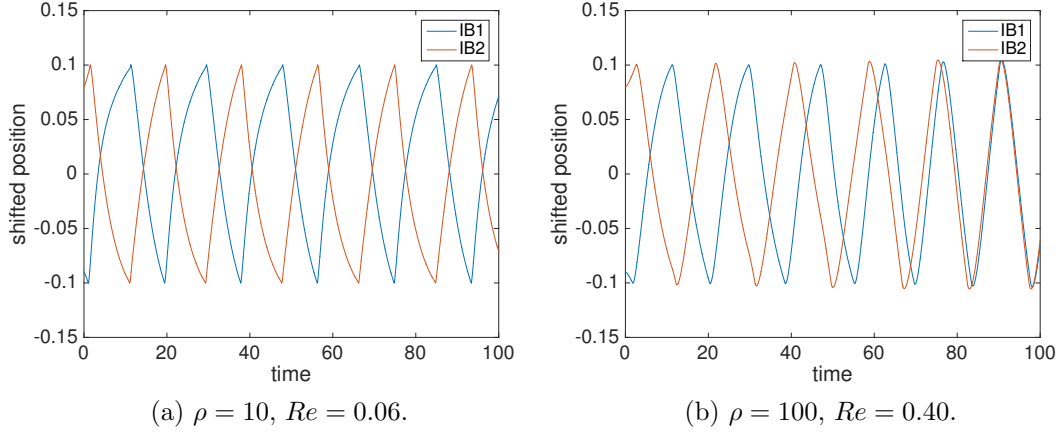


Figure 5.9: Perturbed anti-phase state.

We further run a sequence of perturbations by making

$$x_1 + x_2 = 0, -0.01, -0.02, -0.03, -0.04, -0.05$$

which is from zero perturbation to $0.25(\lambda - 2\xi)$ perturbation, and the corresponding phase diagram is shown in Fig 5.11. The stability region of the anti-phase state gets smaller as Reynolds number gets larger.

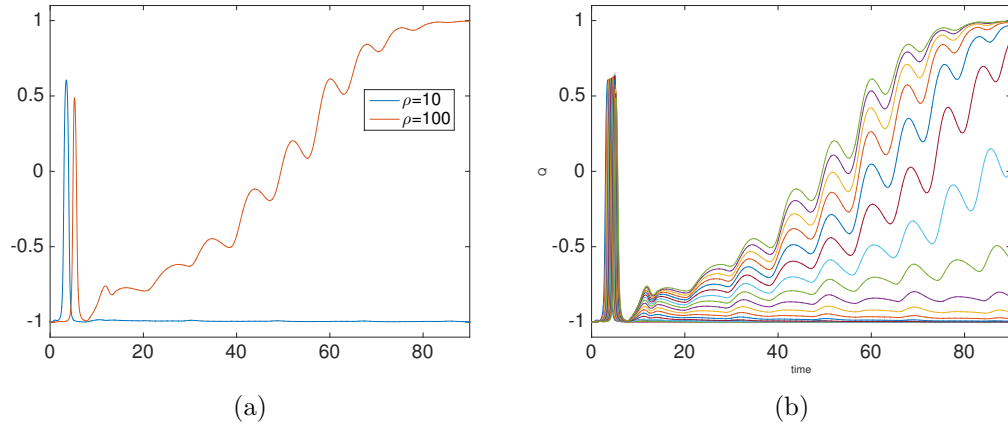


Figure 5.10: Q plot. (a) shows Q plot for $\rho = 10$ ($Re = 0.06$) and $\rho = 100$ ($Re = 0.40$). (b) shows Q plot for $10 \leq \rho \leq 100$ ($0.06 \leq Re \leq 0.40$), with difference of 5 in ρ between each simulation.

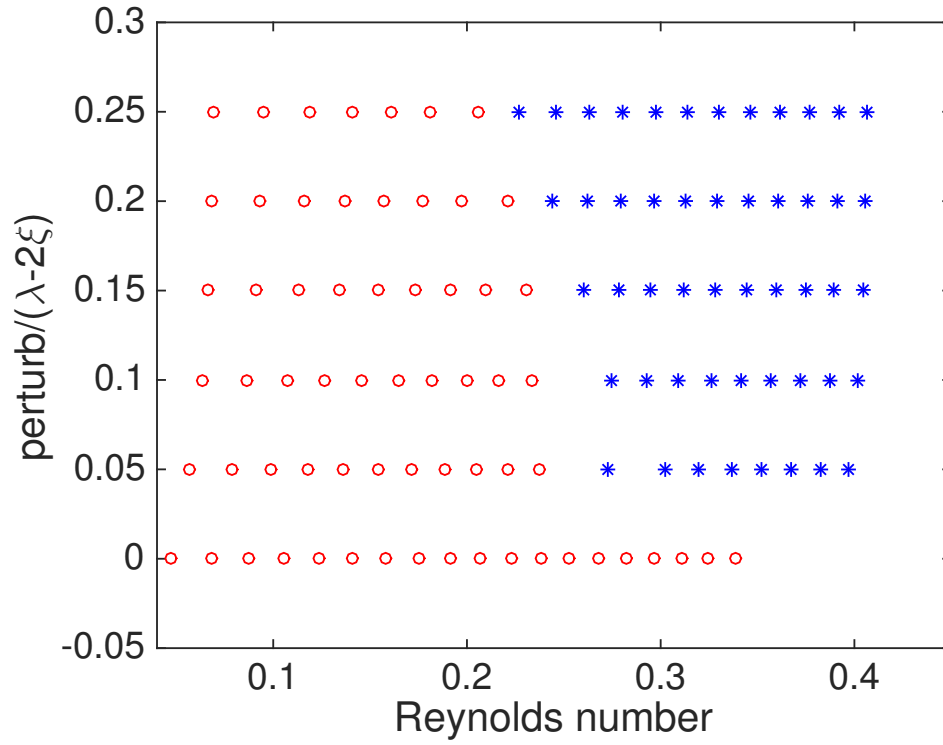


Figure 5.11: Blue star indicates anti-phase unstable, red circle indicates anti-phase stable.

5.4.3 High Re case

Fig 5.12 shows a sequence of snapshots of two oscillators at a higher Reynolds number, $Re = 40.9$. Here we see that the perturbed anti-phase position goes to an in-phase state. Also note that the immersed oscillator experience significant deformation.

5.5 Multiple Oscillators

Here we present a simulation of multiple oscillators coupled through the fluid. An illustration of the initial setting of four oscillators is shown in Fig 5.13. Four oscillators are placed on the vertices of a square, and the initial setting of active trap positions and oscillator positions is randomly generated. Fig 5.14 shows the centroid plot of the four oscillators with all of them shifted to move between -0.1 and 0.1 . All four oscillators synchronize in-phase. The snapshots of the transition from random initial position to in-phase state is shown in Fig 5.15, and a larger snapshot of initial and end velocity field is shown in Fig 5.16.

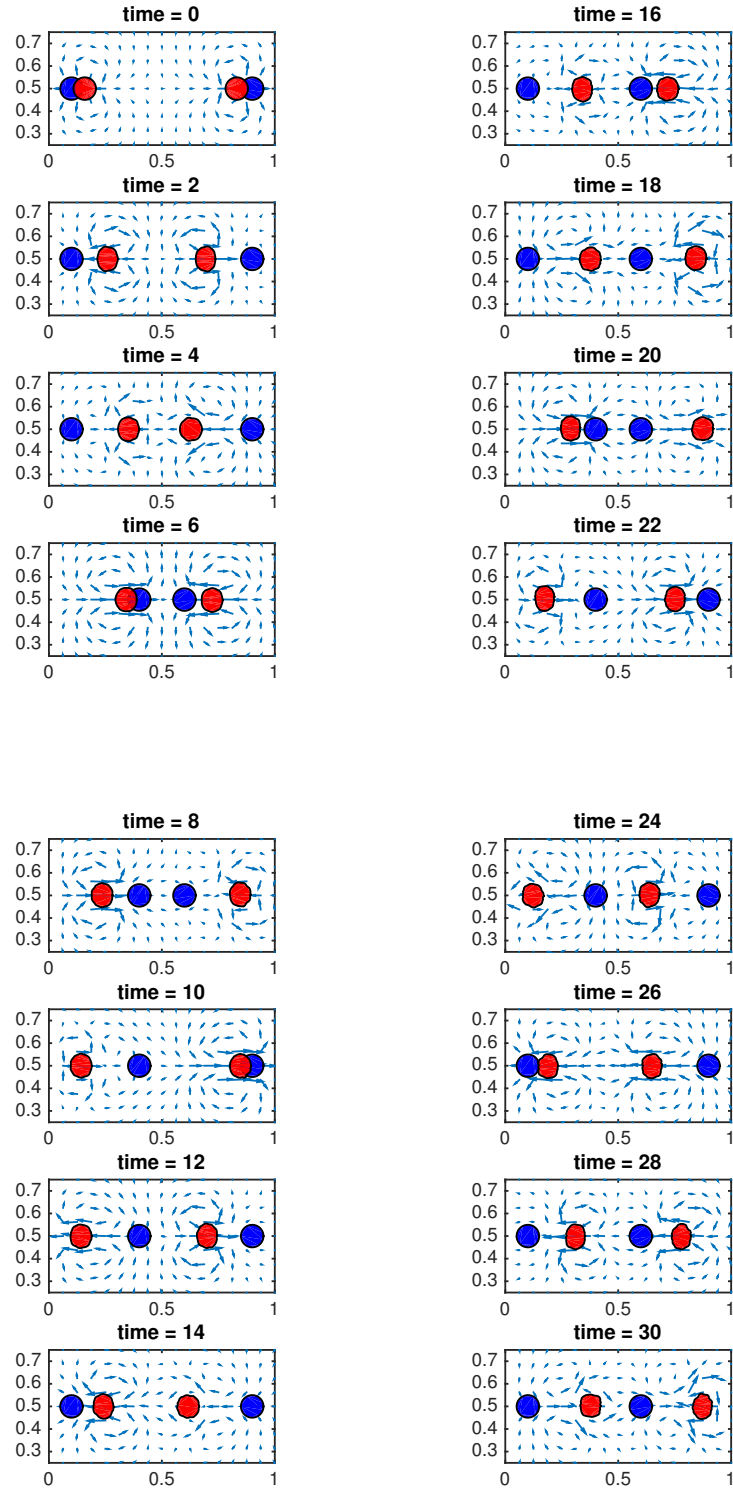


Figure 5.12: For $Re = 40.1$, the coupling state of two oscillators is in-phase, and the deformation is observed.

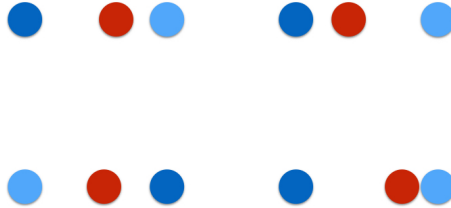


Figure 5.13: Illustration graph for four oscillators coupling.

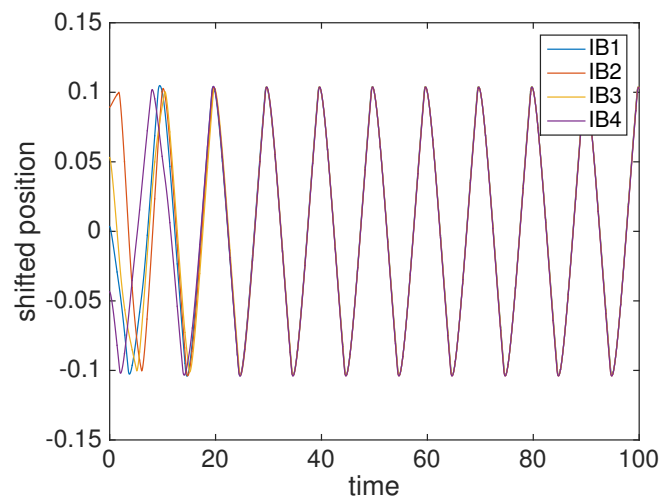


Figure 5.14: Centroid plot for four oscillators. $Re = 0.14$, $\rho = 20$

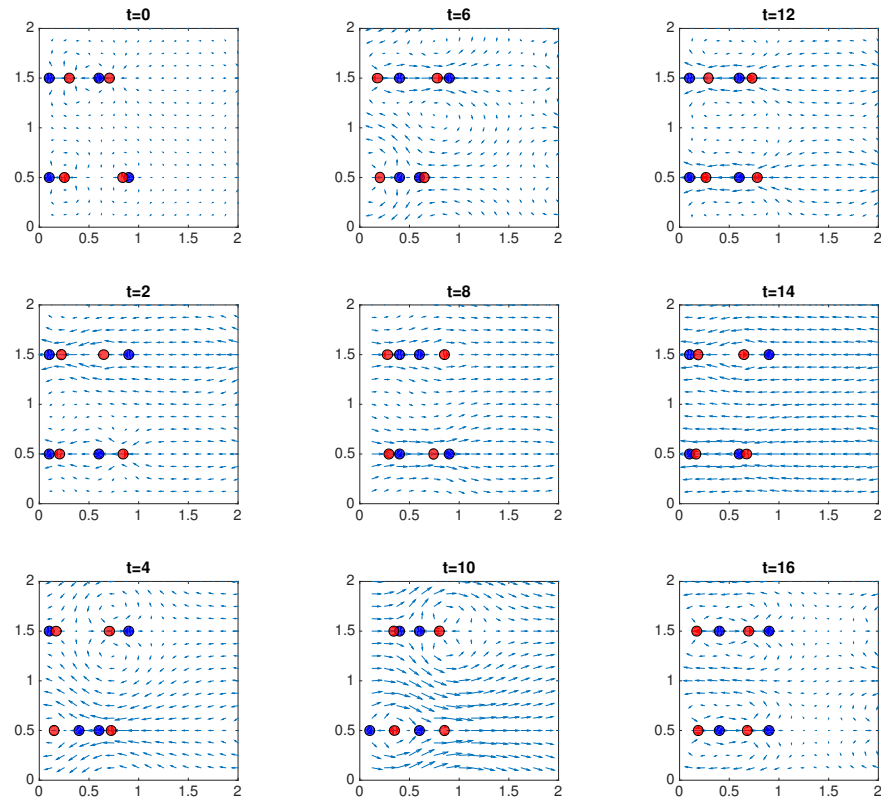


Figure 5.15: Snapshots of four oscillators coupled through fluid.

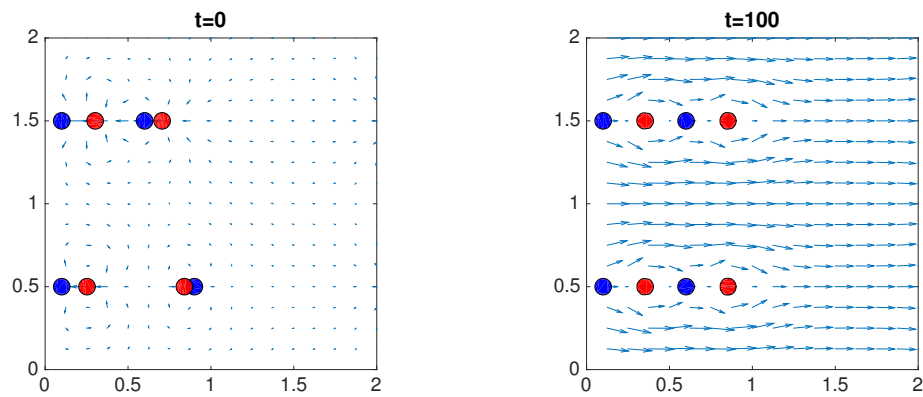


Figure 5.16: Random placed oscillators become in-phase at the end of simulation time.

Chapter 6

Conclusion and Future Work

6.1 Conclusion

In this dissertation, we considered the hydrodynamic interaction between immersed colloidal bodies and a surrounding fluid. We studied the synchronization of these oscillators.

6.1.1 Stokes fluid

For oscillators immersed in a Stokes fluid, we numerically compute the temporal period of a single oscillator using the method of regularized Stokeslets and have the following results:

- The temporal period obtained from the numerical simulation is the same as that obtained from an Oseen tensor approximation analytically.
- For singly-periodic boundary conditions, two cases are studied. If the oscillation direction is the same as the spatial periodicity, the temporal period of the oscillation is longer than the case of single oscillator in free space. If the oscillation direction is orthogonal to the spatial periodicity, the temporal period of the oscillation is shorter than the case of the single oscillator in free space.

Kotar et. al. [4] showed that there are two equilibrium for the motion of two oscillators placed side-by-side: in-phase (unstable) and anti-phase (stable). We validated their result analytically and numerically, and also extended this to other possible settings of oscillators numerically:

- If two oscillators are placed side-by-side and initialized in-phase, the simulated oscillators do not remain in-phase.
- If two oscillators are vertically placed and initialized in-phase, the simulated oscillators remain in-phase. Small perturbations break the equilibrium and make the oscillators become anti-phase quickly.

We study the case where three immersed bodies are placed along the same line and the oscillating direction is same as the line. We showed that by adding a third oscillator to the two oscillator system, the coupling state of the original two oscillators changed from anti-phase to in-phase.

6.1.2 Navier-Stokes fluid

We extend the simulation of hydrodynamic interactions to a Navier-Stokes fluid and study how inertia affects the coupling of oscillators. By using the immersed boundary method to simulate the fluid-structure interaction, we have the following results:

- The temporal period for a single oscillator in a doubly periodic Navier-Stokes fluid is longer than the period of a single oscillator in a free space Stokes fluid. As the spatial periodicity increases, the temporal period decreases.
- Overshooting and deformation of oscillators are observed as Reynolds number gets larger.

We study the cases of two oscillators placed side-by-side. We have shown that because inertia smooths the velocity field in time, oscillators initialized exactly in-phase and anti-phase state remain in their original state. For perturbed in-phase and anti-phase states, we have

- The attraction region for anti-phase state gets smaller as Re gets larger.
- The attraction region for in-phase state gets larger as Re gets larger.

6.2 Future Work

We propose to:

- Change the setting of the two oscillators in the Navier-Stokes fluid to explore synchrony when the orientation of oscillators are varied.
- Study coupled oscillators in a non-Newtonian fluid. By immersing the oscillators in a viscoelastic fluid, the coupling dynamics may differ from our study in a Newtonian fluid .
- Study multiple oscillators in a Navier-Stokes fluid. We only showed one case of more than two oscillators coupled in a Navier-Stokes fluid. Further work will vary Re and the positions, oscillation directions, and numbers of oscillators in the fluid.

Bibliography

- [1] D. M. Woolley, R. F. Crockett, W. D. I. Groom, and S. G. Revell. A study of synchronisation between the flagella of bull spermatozoa, with related observations. *J. Exp. Biol.*, 212(14):2215–2223, 2009.
- [2] R. E. Goldstein, M. Polin, and I. Tuval. Noise and synchronization in pairs of beating eukaryotic flagella. *Phys. Rev. Lett.*, 103:168103, Oct 2009.
- [3] J. Raidt, J. Wallmeier, R. Hjeij, J. G. Onnebrink, P. Pennekamp, N. T. Loges, H. Olbrich, K. Häffner, G. W. Dougherty, H. Omran, and C. Werner. Ciliary beat pattern and frequency in genetic variants of primary ciliary dyskinesia. *Eur. Respir. J.*, 44(6):1579–1588, 2014.
- [4] J. Kotar, M. Leoni, B. Bassetti, M. C. Lagomarsino, and P. Cicuta. Hydrodynamic synchronization of colloidal oscillators. *Proc. Natl. Acad. Sci. USA*, 107(17):7669–7673, 2010.
- [5] H. C. Berg. How to track bacteria. *Rev. Sci. Instrum.*, 42(6), 1971.
- [6] H. C. Berg and R. A. Anderson. Bacteria swim by rotating their flagellar filaments. *Nature*, 245(5425):380–382, 10 1973.
- [7] V. F. Geyer, F. Jülicher, J. Howard, and B. M. Friedrich. Cell-body rocking is a dominant mechanism for flagellar synchronization in a swimming alga. *Proc. Natl. Acad. Sci. USA*, 110(45):18058–18063, 2013.
- [8] G. S. Klindt and B. M. Friedrich. Flagellar swimmers oscillate between pusher- and puller-type swimming. *Phys. Rev. E*, 92:063019, Dec 2015.
- [9] L. Gheber and Z. Priel. Synchronization between beating cilia. *Biophys. J.*, 55(1):183 – 191, 1989.
- [10] A. Vilfan and F. Jülicher. Hydrodynamic flow patterns and synchronization of beating cilia. *Phys. Rev. Lett.*, 96:058102, Feb 2006.
- [11] N. Bruot and P. Cicuta. Realizing the physics of motile cilia synchronization with driven colloids. *Annu. Rev. Condens. Matter Phys.*, 7(1):323–348, 2016.
- [12] L. A. Hough and H. D. Ou-Yang. Correlated motions of two hydrodynamically coupled particles confined in separate quadratic potential wells. *Phys. Rev. E*, 65:021906, Jan 2002.

- [13] S. Herrera-Velarde, E. C. Eun-Daz, F. Crdoba-Valds, and R. Castaeda-Priego. Hydrodynamic correlations in three-particle colloidal systems in harmonic traps. *J. Phys. Condens. Matter*, 25(32):325102, 2013.
- [14] M. Leoni, J. Kotar, B. Bassetti, P. Cicuta, and M. C. Lagomarsino. A basic swimmer at low reynolds number. *Soft Matter*, 5:472–476, 2009.
- [15] R. Lhermerout, N. Bruot, G. M. Cicuta, J. Kotar, and P. Cicuta. Collective synchronization states in arrays of driven colloidal oscillators. *New J. Phys.*, 14(10):105023, 2012.
- [16] G. M. Cicuta, J. Kotar, A. T. Brown, J.-H. Noh, and P. Cicuta. Hydrodynamic coupling in polygonal arrays of colloids: Experimental and analytical results. *Phys. Rev. E*, 81:051403, May 2010.
- [17] L. Damet, G. M. Cicuta, J. Kotar, M. C. Lagomarsino, and P. Cicuta. Hydrodynamically synchronized states in active colloidal arrays. *Soft Matter*, 8:8672–8678, 2012.
- [18] G. M. Cicuta, E. Onofri, M. C. Lagomarsino, and P. Cicuta. Patterns of synchronization in the hydrodynamic coupling of active colloids. *Phys. Rev. E*, 85:016203, Jan 2012.
- [19] N. Bruot, J. Kotar, F. de Lillo, M. Cosentino Lagomarsino, and P. Cicuta. Driving potential and noise level determine the synchronization state of hydrodynamically coupled oscillators. *Phys. Rev. Lett.*, 109:164103, Oct 2012.
- [20] R. G. W. Mario Theers. Effects of thermal fluctuations and fluid compressibility on hydrodynamic synchronization of microrotors at finite oscillatory reynolds number: a multiparticle collision dynamics simulation study. *Soft Matter*, 10(32):5894–5904, 2014.
- [21] S. M. Block. Making light work with optical tweezers. *Nature*, 360(6403):493–495, 12 1992.
- [22] R. Cortez. The method of regularized stokeslets. *SIAM J. Sci. Comput.*, 23(4):1204–1225, 2001.
- [23] H. Lamb. *Hydrodynamics*. Dover, 6 edition, 1932.
- [24] F. Mannan and R. Cortez. The method of regularized stokeslets in a two-dimensional domain with one periodic direction. In preparation.
- [25] C. S. Peskin. Flow patterns around heart valves: A numerical method. *J. Comput. Phys.*, 10(2):252 – 271, 1972.
- [26] C. S. Peskin. The immersed boundary method. *Acta Numer.*, 11:479–517, 1 2002.

- [27] A. L. Fogelson and C. S. Peskin. A fast numerical method for solving the three-dimensional stokes' equations in the presence of suspended particles. *J. Comput. Phys.*, 79(1):50 – 69, 1988.
- [28] E. Lauga and T. R. Powers. The hydrodynamics of swimming microorganisms. *Rep. Prog. Phys.*, 72(9):096601, 2009.
- [29] J. M. Teran and C. S. Peskin. Tether force constraints in stokes flow by the immersed boundary method on a periodic domain. *SIAM J. Sci. Comput.*, 31(5):3404–3416, 2009.

Biography

The author was born in Tianjin, China in 1988 and graduated from University of Science and Technology of China with a Bachelor degree in Applied Mathematics in 2010. The author started the PhD program at the Tulane University mathematics department in August 2010, eventually completing the program in August 2016.